Biochemistry and Chemical Biology
Microbiology and Infectious Disease

A General Mechanism for Initiating the General Stress Response in Bacteria

Reviewed Preprint
v2 • April 3, 2025
Revised by authors

Reviewed Preprint
v1 • September 12, 2024

Rishika Baral, Kristin Ho, Ramasamy P Kumar, Jesse B Hopkins, Maxwell B Watkins, Salvatore LaRussa, Suhaily Caban-Penix, Logan A Calderone, Niels Bradshaw

Department of Biochemistry, Brandeis University, Waltham, United States • Graduate program in Biochemistry and Biophysics, Brandeis University, Waltham, United States • Biophysics Collaborative Access Team (BioCAT), Department of Physics, Illinois Institute of Technology, Chicago, United States • Biophysics Collaborative Access Team (BioCAT), Department of Biology, Illinois Institute of Technology, Chicago, United States • Graduate program in Molecular and Cell Biology, Brandeis University, Waltham, United States

eLife Assessment

This **important** study combines genetic analysis, biochemistry, and structural modeling to reveal new insights into how changes in protein-protein structure activate signal transduction as part of the bacterial general stress response. The data, which was collected using validated and standard methods, and its interpretations are **convincing**; however, to fully meet the title's promise, additional experimental evidence is needed to strengthen the proposed model and its potential application to other systems. This manuscript will be of broad interest to microbiologists, structural biologists, and cell biologists.

https://doi.org/10.7554/eLife.100376.2.sa4

Abstract

The General Stress Response promotes survival of bacteria in adverse conditions, but how sensor proteins transduce species-specific signals to initiate the response is not known. The serine/threonine phosphatase RsbU initiates the General Stress Response in *B. subtilis* upon binding a partner protein (RsbT) that is released from sequestration by environmental stresses. We report that RsbT activates RsbU by inducing otherwise flexible linkers of RsbU to form a short coiled-coil that dimerizes and activates the phosphatase domains. Importantly, we present evidence that related coiled-coil linkers and phosphatase dimers transduce signals from diverse sensor domains to control the General Stress Response and other signaling across bacterial phyla. This coiled-coil linker transduction mechanism additionally suggests a resolution to the mystery of how shared sensory domains control serine/threonine phosphatases, diguanylate cyclases and histidine kinases. We propose that this provides bacteria with a modularly exchangeable toolkit for the evolution of diverse signaling pathways.

Introduction

The General Stress Response (GSR) allows bacteria to survive in hostile and changing environments(Bergkessel et al. 2016; Harms et al. 2016; Gottesman 2019; Guldimann et al. 2016; Hecker et al. 2007). A defining feature of the GSR is that it controls transcription of a large and diverse set of genes, dramatically reshaping the physiology of the organism (Gottesman 2019; Guerreiro et al. 2020; Boekhoud et al. 2020; Boylan et al. 1993). Another defining feature is that the GSR is induced by a variety of stress conditions that are frequently associated with each other, including stationary phase, nutrient depletion, cellular damage, and (for pathogens) host defense mechanisms (Gottesman 2019). This multiplicity of initiating conditions allows cells to anticipate and prepare for accumulating adversity, suggesting why the GSR is present in every bacterial species that has so far been analyzed. The GSR additionally contributes to pathogenesis through expression of genes controlling virulence, biofilm formation, and quorum sensing (Kint et al. 2017; Battesti et al. 2015; Bartolini et al. 2019). Inactivation of the GSR, in turn, promotes the transition to long-term slow growth and antibiotic resistance, which are particularly important for persistent infections (Tuchscherr & Löffler 2016; Herbert et al. 2010; Bergkessel et al. 2016). Thus, deciphering the mechanisms that govern GSR activity is critical to understanding how bacteria interact with and adapt to their environments.

A major barrier to understanding initiation of the GSR is that we lack a unique, generalizable mechanistic model for how the activating signaling proteins have evolved to respond to species-specific signals. In a widespread mechanism for initiating the GSR, a member of the PPM family of serine/threonine phosphatases dephosphorylates a phosphorylated substrate protein to activate an alternative σ-factor through a “partner-switching” mechanism (Hecker et al. 2007), but how the phosphatase receives and is activated by an upstream signal has not been determined.

In this study, we address how the GSR phosphatase RsbU from *B. subtilis* is regulated (Yang et al. 1996) and present evidence that this mechanism is widely conserved. RsbU dephosphorylates a single phospho-serine on its substrate protein (RsbV) to release the GSR transcription factor (σ^B) from inhibition by an anti-sigma factor (RsbW) (**Figure 1A**). RsbU has an N-terminal four-helix bundle domain that dimerizes RsbU and is also the binding site for RsbT, which activates RsbU as a phosphatase (**Figure 1C,D**) (Delumeau et al. 2004). RsbT is sequestered in a megadalton stress sensing complex called the stressosome, and is released to bind RsbU in response to specific stress signals including ethanol, heat, acid, salt, and blue light (Hecker et al. 2007; Marles-Wright et al. 2008). We and others have reconstituted RsbU activation by RsbT (Delumeau et al. 2004; Ho & Bradshaw 2021), but how RsbT activates RsbU was not known.

This “partner-switching” mechanism is broadly conserved, and the activating phosphatases are observed to have diverse N-terminal sensory domains including PAS (Vijay et al. 2000; Greenstein et al. 2009; Fernández Martínez et al. 2009), response-receiver (de Been et al. 2010; Rodríguez-Martínez et al. 2023), GAF (Kint et al. 2019), and HAMP (Mittenhuber 2002). These signaling domains are frequently found as N-terminal regulators of histidine kinases and GGDEF diguanylate cyclases in bacteria, but whether or not there are shared mechanistic features between the regulatory principles of PPM phosphatases and these other signaling effector families is not known (Möglich et al. 2009; Galperin 2006).

We previously described a mechanism for allosteric control of the related *B. subtilis* phosphatase SpoIIE, which regulates endospore formation through a partner-switching mechanism analogous to RsbU control of the GSR (Ho & Bradshaw 2021; Bradshaw et al. 2017). Two helices of the PPM domain (α1 and α2), which we refer to as the switch element, change conformation to recruit metal cofactor and activate SpoIIE (Bradshaw et al. 2017). Based on analysis of structural and genetic data, we conjectured that this conformational change exemplifies a common mechanism

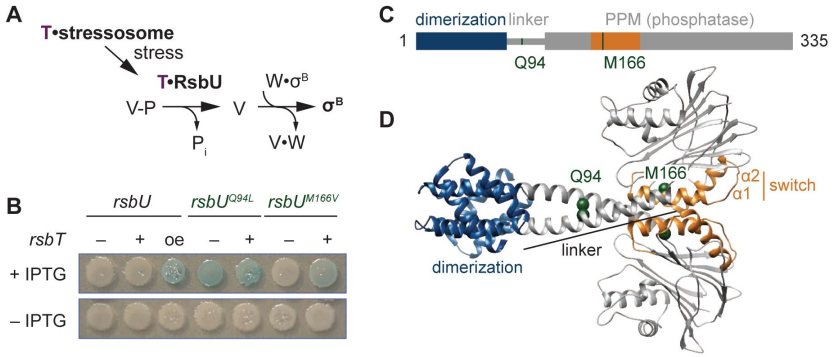

Figure 1

The linker controls RsbU activation through a conserved switch element

A Reaction scheme of the RsbU dependent pathway of the environmental stress response. RsbU is activated by its partner protein RsbT (T, purple) to dephosphorylate its substrate protein RsbV-P (V-P). This initiates transcription by displacing σ^B from inhibition by the anti-sigma factor RsbW (W). **B** Amino acid substitutions in RsbU (Q94L and M166V) cause enhanced σ^B activity in *B. subtilis*. Strains carrying a lacZ reporter of σ^B activity (*ctc-lacZ*) were plated on X-gal indicator plates in the presence (top) or absence (bottom) of IPTG to induce expression of the rsbU constructs. Strains were deleted for *rsbT* (–) or not (+). A strain overex-pressing *rsbT* is indicated by oe. Plates were imaged after 24 hours of growth at 37°C, which was shorter than the time used to visualize *lacZ* expression from the *rsbU*^{M166V} strain previously (Ho & Bradshaw 2021). **C** Domain diagram of RsbU. The N-terminal domain of RsbU (blue) (amino acids 1-81) is joined to the α-helical linker domain (grey) (82-112), which connects it to the PPM phosphatase domain (grey box) (121-335). The regulatory switch element of the PPM phosphatase domain is colored orange (156-201). The location of RsbT-bypass mutations are highlighted in green. **D** AlphaFold2 model of RsbU dimer. Domains are colored as in C and the Cα atoms of residues Q94 and M166 are shown as spheres.

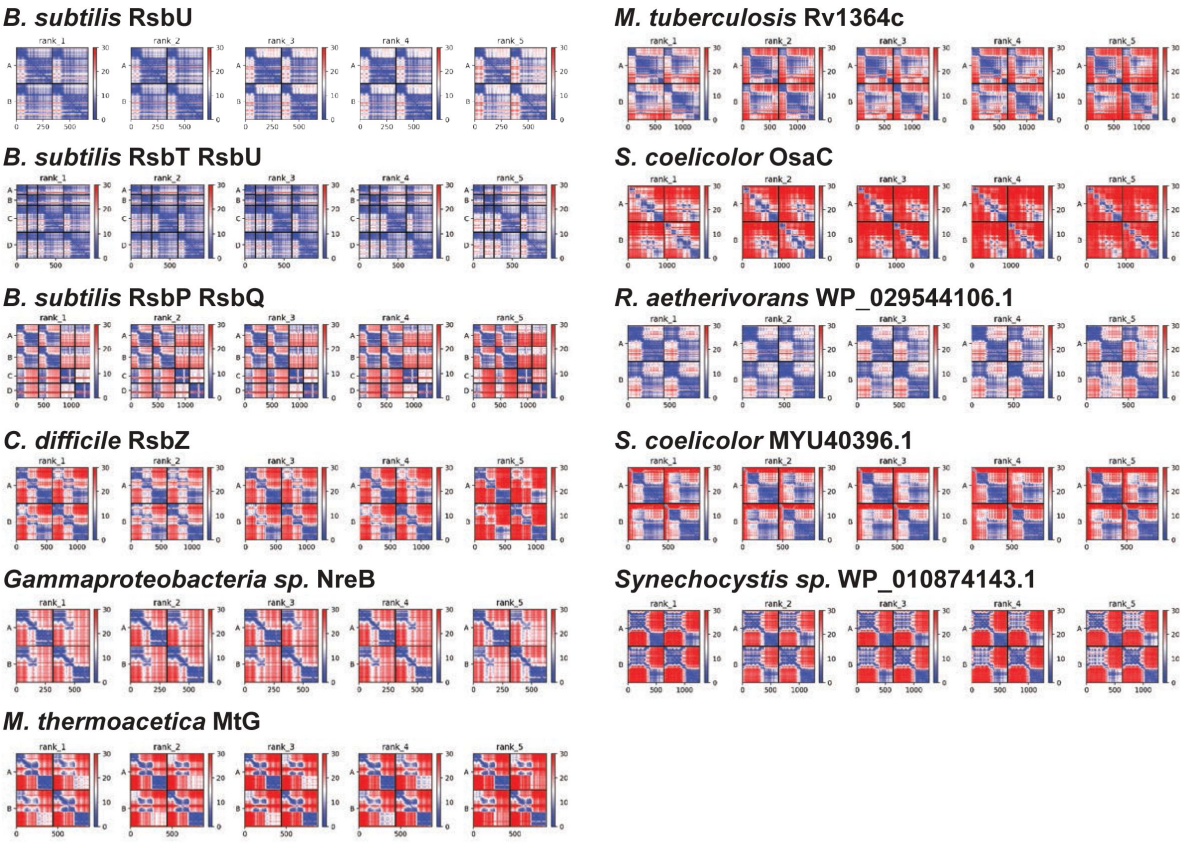

Figure 1 - Supplemental Figure 1

PAE plots of AlphaFold2 prediction

Predicted aligned error of the AlphaFold2 structure predictions of the following proteins: B. subtilis RsbU, *B. subtilis* 2RsbT (chains A, B)/2RsbU (chains C,D) complex, *B. subtilis* 2RsbP (chains A,B)/2RsbQ complex (chains C,D), *C. difficile* RsbZ, *Gammaproteo-bacteria sp.* NreB, *M. thermoacetica* MtG, *M. tuberculosis* Rv1364c, *S. coelicolor* OsaC, *R. aetherivorans* WP_029544106.1, *S. coelicolor* MYU40396.1, and *Synechocystis sp.* WP_010874143.1. Blue indicates high confidence (0 Å) and red indicates low confidence (30 Å).

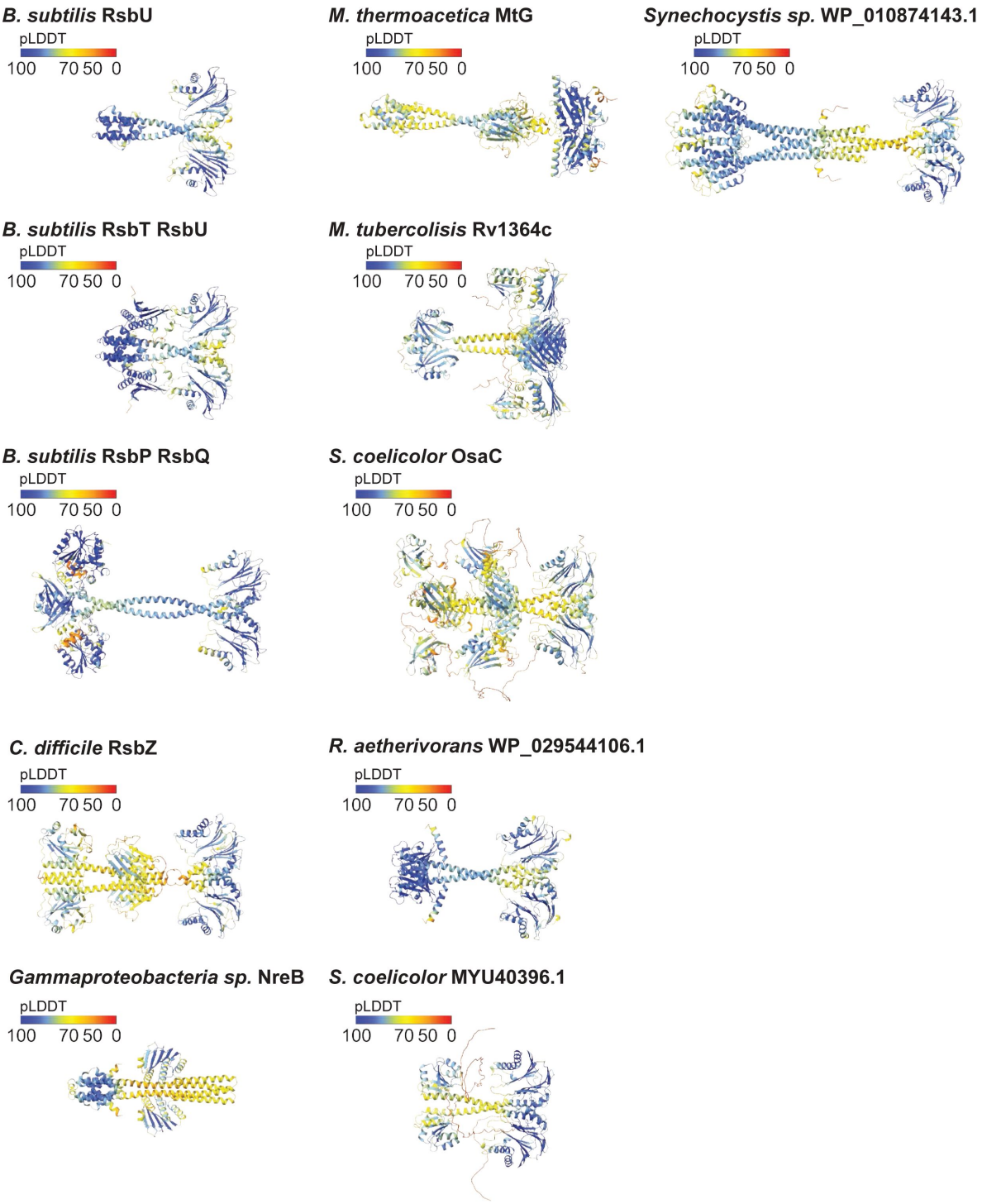

Figure 1 - Supplemental Figure 2

AlphaFold2 structure predictions with mapped pLDDT scores

Predicted local distance difference test scores (pLDDT) mapped onto the AlphaFold2 structure predictions of the following proteins: *B. subtilis* RsbU, *B. subtilis* 2RsbT/2RsbU complex, *B. subtilis* 2RsbP/2RsbQ complex, *C. difficile* RsbZ, *Gammaproteobacteria sp.* NreB, *M. thermoacetica* MtG, *M. tuberculosis* Rv1364c, *S. coelicolor* OsaC, *R. aetherivorans* WP_029544106.1, *S. coelicolor* MYU40396.1, and *Synechocystis sp.* WP_010874143.1. The score key is above each structure model. Blue corresponds to a pLDDT score of 90-100 (high confidence), orange to yellow corresponds to a pLDDT score of 50-70 (medium confidence), and red corresponds to a pLDDT score of 0 (low confidence).

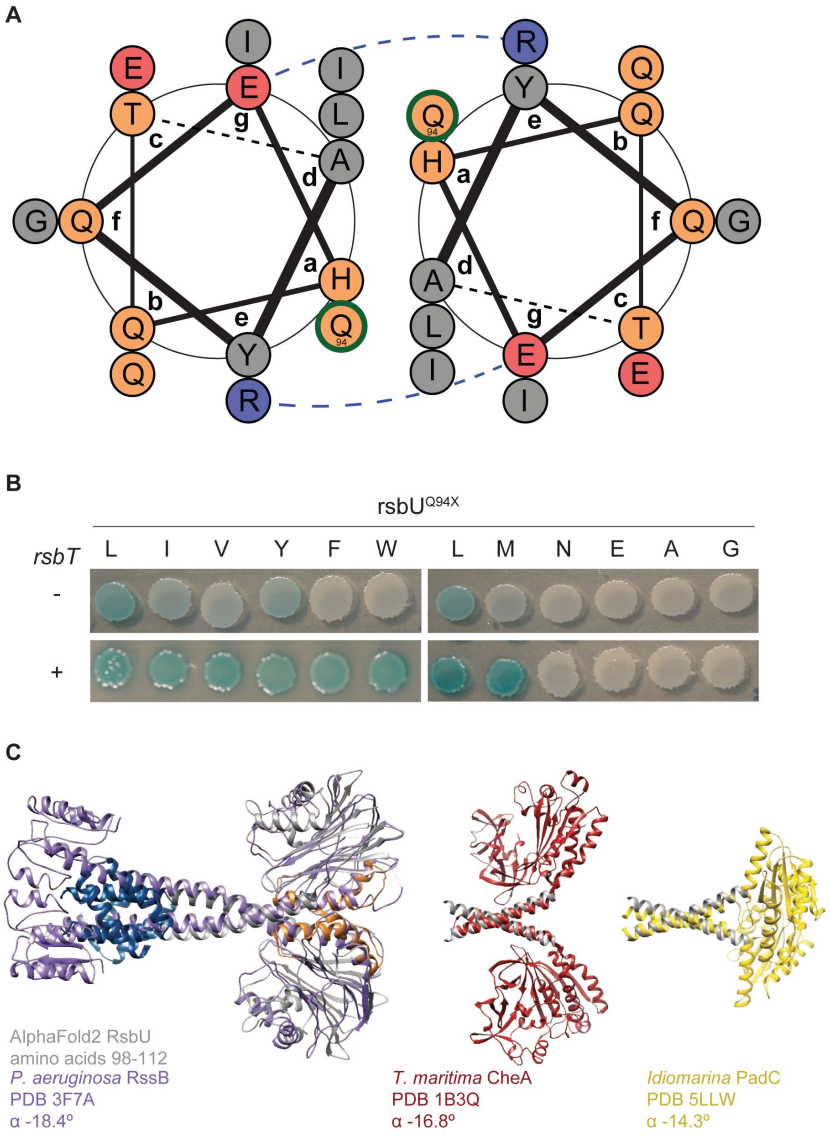

Figure 1 - Supplemental Figure 3

Q94L stabilizes the packing interface of the coiled-coil of the linker

A Coil diagram of RsbU residues 83-97 generated using DrawCoil. Grey circles indicate non-polar residues, orange indicate polar residues, red indicate negatively charged residues, and blue indicate positively charged residues. The blue dashed line depicts a putative salt bridge. Residue Q94 (circled in green) sits in the interface of the coils and is shown packing with L90. **B** An allelic series of amino acid substitutions at position 94 of RsbU was generated in an *rsbU* expression plasmid. Plasmids were introduced into *B. subtilis* cells containing a LacZ reporter of σ^B activity that were deleted for *rsbT* (top) or with *rsbT* retained on the chromosome (bottom). Cells were plated on IPTG/X-gal plates to induce *rsbU* expression and to indicate σ^B activity (blue pigmentation). **C** α-helical pitch analysis of coiled-coil domains. The AlphaFold2 model of an RsbU dimer is overlayed with crystal structure of *P. aeruginosa* RssB (PDB 3F7A, purple, left). The helical linker region extending out of the coiled coil (RsbU98-112) is shown (grey) overlaid with *T. maritima* transducing histidine kinase CheA (PDB 1B3Q, red, middle) and *Idiomarina* A28L diguanylyl cyclases PadC (PDB 5LLW, yellow, right). α angles from Crick parameterization analysis using CCCP are shown for the overlaid region.

among diverse phosphatases. However, we could not propose a specific model for how unrelated regulatory domains modularly control the switch conformation. For RsbU, we found that RsbT enhances phosphatase activity by increasing the efficacy of metal cofactor binding and that substitution of an amino acid in α1 ($RsbU^{M166V/L}$) activates RsbU in the absence of RsbT (Ho & Bradshaw 2021) These results supported our proposal that the switch element controls RsbU activation, but they did not reveal how RsbT binding to the N-terminus of RsbU is transduced to the switch.

One broadly conserved feature of GSR phosphatases (absent in SpoIIE) is an α-helical linker of variable length, which is N-terminal to the PPM phosphatase domain. Genetic data suggest that this linker regulates a paralogous *B. subtilis* GSR phosphatase (RsbP) (Brody et al. 2009). Here we report that binding of RsbT to the N-terminus of RsbU rigidifies an otherwise flexible linker to dimerize the C-terminal phosphatase domains through an interface mediated by the switch element. Importantly, and as we now report, this mechanism is generalizable to other PPM phosphatases and reveals a widespread feature of bacterial signaling.

Results

The linker controls RsbU activation through a predicted phosphatase dimer

We previously conducted a genetic screen (Ho & Bradshaw 2021) to identify features of RsbU that are important for phosphatase regulation by isolating gain-of-function variants that are active in the absence of RsbT. Focusing on the phosphatase domain in our initial study, we reported identification of an amino acid substitution in α1 ($RsbU^{M166V/L}$) that links the switch element to RsbU activation (Ho & Bradshaw 2021). From this screen, we isolated a second variant, $RsbU^{Q94L}$, located in the linker of RsbU between the N-terminal dimerization domain and the C-terminal phosphatase domain (**Figure 1B-D**). *rsbU*^{Q94L}strains activated σ^B in the absence of *rsbT*. This activation is comparable to when *rsbT* is overexpressed to exceed the capacity of the stressosome and is stronger than what we observe in strains expressing *rsbU*$^{M166V/L}$ (**Figure 1B**).

To visualize how the Q94L and M166V/L substitutions could impact RsbU structure and activity, we generated an AlphaFold2 model of an RsbU dimer (Jumper et al. 2021; Mirdita et al. 2022) (**Figure. 1D**). The prediction of the complex was of high confidence (**Figure 1 - figure Supplement 1-2**) and had a dimer of the N-terminal region consistent with a previous experimental structure (Delumeau et al. 2004). In our model, the linkers form extended alpha-helices (82-112) that cross to connect dimers of the RsbU N-terminal domains and C-terminal phosphatase domains, with Q94 buried in the linker interface and M166 buried in the core of the phosphatase domain (**Figure 1D**).

The crossing linker helices have similar conformation to homologous linkers observed in crystal structures of *P. aeruginosa* RssB, a phosphatase/adapter protein that also controls the GSR (PDB 3F7A and 3EQ2, **Figure 1 – Figure Supplement 3**). RssB has an N-terminal response-receiver domain in place of the RsbU four helix bundle dimerization domain, suggesting that linker conformation is a conserved feature of PPM phosphatase dimers with divergent N-terminal regulatory domains (**Figure 1 – Figure Supplement 3**). The linker helices in the RsbU prediction and the RssB structure splay apart as they enter the PPM domain with similar angle (pitch angles (α) based on Crick parameters for coiled-coils –17.6° and –18.4° respectively) and pack against α-1 of the PPM fold (Grigoryan & DeGrado 2011). Interestingly, we observed that other bacterial signaling proteins that are regulated by coiled-coil linkers had similar pitch angle for the helices connecting to the catalytic domains (for example the dimeric histidine kinase CheA, 1B3Q, α –16.8°, and the dimeric GGDEF diguanylate cyclase PadC, 5LLW, α –14.3°) (Bilwes et al. 1999; Gourinchas

et al. 2017; Grigoryan & DeGrado 2011) (**Figure 1 – Figure Supplement 3**). Thus, the linker of RsbU could be a conserved regulatory feature, analogous to linkers of histidine kinases and GGDEF diguanylate cyclases.

Analysis of the RsbU dimer model using Socket2 identifies amino acids 83-97 as a two-turn coiled coil, with Q94 unfavorably packing against leucine 90 (Kumar & Woolfson 2021) (**Figure 1 – Figure Supplement 3**). To test whether hydrophobicity at position 94 promotes an active state, we tested the activity of RsbU alleles with different amino acid substitutions at position 94 for σ^B in wildtype and *rsbT* deleted strains. We found that substitutions of Q94 with amino acids that could pack at the intersection of the crossing linker helices (hydrophobic residues isoleucine, valine, and methionine, as well as tyrosine) resulted in mild, RsbT-independent activation of σ^B that was further heightened by RsbT (**Figure 1 – Figure Supplement 3**). Aromatic hydrophobic residues (phenylalanine and tryptophan) drove constitutive activation of RsbU but did not bypass the requirement for *rsbT* on the chromosome (**Figure 1 – Figure Supplement 1**). Substitutions of small or charged residues (alanine, glycine, glutamate, and asparagine) did not lead to activity in either strain (**Figure 1 – Figure Supplement 3**). These results are consistent with a model in which burial of the amino acid at position 94, such as in the crossed helices of our prediction for RsbU dimer structure, drives RsbU activation.

RsbT binding to RsbU is influenced by the linker

One prediction of our hypothesis that RsbT stabilizes the crossed alpha helices of the RsbU dimer, is that RsbT should bind more tightly to $RsbU^{Q94L}$ than to RsbU because the coiled-coil conformation that RsbT binds would be more energetically favorable. To test this, we measured the binding affinity of RsbT for RsbU using fluorescence anisotropy. From these data we obtained a K_D of 4.5 ± 1 μM, which decreased approximately 10-fold for $RsbU^{Q94L}$ (0.56 ± 0.2 μM) (**Figure 2A**). Thus, $RsbU^{Q94L}$ stimulates RsbU phosphatase activity by an on-pathway mechanism, supporting the idea that RsbT binding stabilizes the linker in a dimerized conformation to activate RsbU.

RsbU phosphatase activation is controlled by the linker

We previously found that RsbT activates RsbU by simultaneously decreasing the K_M for manganese cofactor and increasing the k_{cat} for dephosphorylation of RsbV-P (Ho & Bradshaw 2021). To test whether RsbU Q94L substitution works by the same kinetic mechanism, we measured dephosphorylation of ^{32}P-phosphorylated RsbV by $RsbU^{Q94L}$ (**Figure 2B**). The k_{cat} of $RsbU^{Q94L}$ was nearly the same as for the basal activity of RsbU (2.4 ± 0.1 min^{-1} compared to 1.4 ± 0.1 min^{-1}, and stimulated more than ten-fold by RsbT, 15 ± 0.4 min^{-1}) (**Figure 2B**) (Ho & Bradshaw 2021). However, $RsbU^{Q94L}$ had a K_M for $MnCl_2$ (1.4 ± 0.2 mM) that is more than fifty-fold reduced compared to RsbU alone (77 ± 9 mM) (Ho & Bradshaw 2021), and similar to the K_M^{MnCl2} of RsbU in the presence of RsbT (0.98 ± 0.07 mM (Ho & Bradshaw 2021)) (**Figure 2B**). Addition of RsbT did not change the K_M of $RsbU^{Q94L}$ for $MnCl_2$ (1.9 ± 0.6 mM), but the maximum catalytic rate of dephosphorylation increased nearly four-fold to 9.0 ± 0.64 min^{-1}, approaching the rate of RsbU stimulated by RsbT (**Figure 2B**). Thus, $RsbU^{Q94L}$ substantially recapitulates RsbT activation by decreasing the K_M for Mn^{2+}, demonstrating that the linker transduces RsbT binding to control the active site of RsbU (**Figure 2C**). This is consistent with previous findings that the allosteric switch controlling phosphatase activity of SpoIIE couples dimerization to cofactor interaction.

RsbT binds to the linker and N-terminal domain

To visualize how RsbT could control the linker to activate RsbU, we generated an AlphaFold2 prediction of a heterotetrameric complex between RsbT and RsbU (**Figure 3A**). In this model, RsbU adopts a conformation very similar to our prediction of the RsbU dimer (RMSD 1.36 Å), suggesting that our AlphaFold2 RsbU dimer model represents the active state of RsbU even when

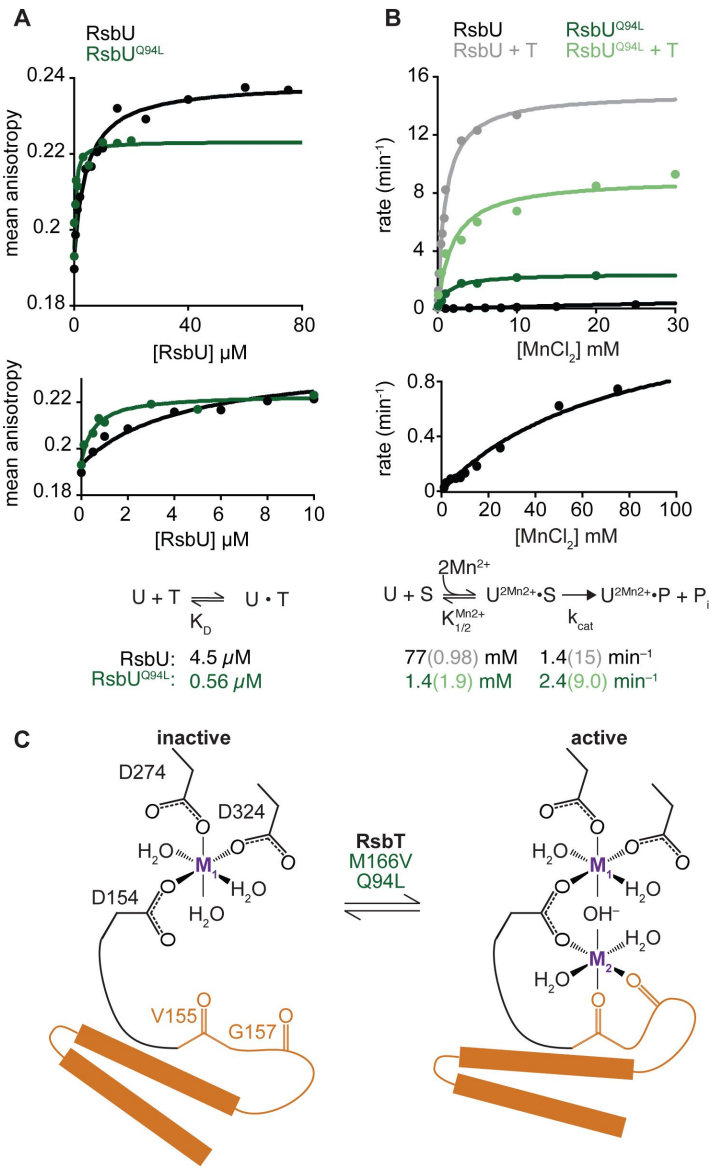

Figure 2

RsbU linker influences RsbT binding and phosphatase activity

A Mean anisotropy of RsbT-TMR (200 nM) is plotted as a function of RsbU concentration. The curves are fits to a quadratic binding equation using non-linear curve fitting (RsbU (black) K_D = 4.5 ± 0.96 μM, $RsbU^{Q94L}$ (green) K_D = 0.56 ± 0.15 μM). The lower plot shows RsbU concentrations to 10 μM. Below is the reaction scheme of RsbT binding to RsbU with the values for the calculated K_D below. **B** The rate of dephosphorylation of RsbV-P is plotted as a function of concentration of $MnCl_2$ for RsbU (black) and $RsbU^{Q94L}$ (green) in the presence (dark) and absence (light) of RsbT. Curves are fits to the Michaelis-Menten equation using non-linear curve fitting. The k_{cat} of wild-type RsbU is 15 ± 0.35 min^{-1} with RsbT and 1.4 ± 0.077 min^{-1} without RsbT and the k_{cat} of $RsbU^{Q94L}$ is 9.0 ± 0.64 min^{-1} with RsbT and 2.4 ± 0.084 min^{-1} without RsbT. The K_M^{MnCl2} of wild-type RsbU is 0.98 ± 0.069 mM with RsbT and 77 ± 9.0 mM without RsbT and the K_M^{MnCl2} of $RsbU^{Q94L}$ is 1.4 ± 0.19 mM with RsbT and 1.9 ± 0.56 mM without RsbT. The lower plot shows wild-type RsbU in the absence of RsbT for $MnCl^2$ concentrations to 100 mM. Below is a summary of a reaction scheme of RsbU dephosphorylating RsbV-P (denoted as S) with the K_M^{MnCl2} and k_{cat} values below. Data for RsbU are reproduced from Ho & Bradshaw 2021. **C** A cartoon model of how the switch helices rotate to activate RsbU. Binding of RsbT or mutation moves the switch helices into place during activation to coordinate metal M2. The residues of RsbU that are hypothesized to coordinate metals are shown as sticks (based on homology to RsbX).

RsbT was not included in the prediction (a known feature of AlphaFold2 models(Chakravarty & Porter 2022). The predicted structure places RsbT in a hybrid interface that spans the N-terminal dimerization domain of both RsbU monomers and the linker of one monomer (**Figure 3A**). Supporting the validity of the AlphaFold2 2RsbT/2RsbU model, residues previously implicated in RsbT/U binding (Hardwick et al. 2007) (Y28 and E24 from one RsbU monomer, I74, and I78 from the other RsbU monomer, and RsbT R19, R23, and N24) are all buried in the predicted interface (**Figure 3 – Figure supplement 1**).

To gain further insight into how RsbT binding is transduced to RsbU linker conformation and phosphatase activity, we performed a genetic screen to isolate suppressors of $RsbU^{Y28I}$, which was previously observed to abolish binding to RsbT (Hardwick et al. 2007). After screening a library of PCR mutagenized $rsbU^{Y28I}$ and *rsbT*, we identified eleven variants that introduced substitutions to RsbU that suppress $rsbU^{Y28I}$: S49G, K53E, T89A, G92E, G92R, Q94L, T110S, V142A, K143E, C165Y, and M173I (**Figure 3A-B**). We additionally isolated revertants that restored Y28 suggesting that the screen was near saturation, but did not isolate any suppressors in *rsbT*, which was also mutagenized.

Mapping the $RsbU^{Y28I}$ suppressor mutations onto our 2RsbU/2RsbT model suggests that they fall into three classes (**Figure 3A** and **B**): *(1)* Substitutions in the RsbU N-terminal dimerization domain that map near the predicted RsbT binding site (S49G and K53E), supporting the predicted interface. *(2)* Substitutions that map near predicted contacts between RsbT and the RsbU linker (T89A, G92E/R, and Q94L), providing evidence that contacts between RsbT and the linker promote RsbU activation. *(3)* Substitutions that cluster around the regulatory switch element of the RsbU phosphatase domain (helices α1 and α2 of the PPM fold, T110S, V142A, K143E, C165Y, and M173I). We hypothesize that these substitutions rescue $RsbU^{Y28I}$ inactivation by reducing the energetic cost (normally provided by RsbT binding) to transition the RsbU phosphatase domain to the active conformation. Together these genetic data provide independent support for the AlphaFold2 model of the 2RsbT/2RsbU complex, and suggest that RsbT activates RsbU by transmitting signals to the switch element in the RsbU phosphatase domain through a coiled-coil linker.

Contacts between RsbT and the RsbU linker drive phosphatase activation

To test the model that RsbT activates RsbU by directly interacting with the linker to dimerize the RsbU phosphatase domains, we introduced a charge swap at position R91 that would abolish a predicted salt-bridge with RsbT D92 (**Figure 3C**). $RsbU^{R91E}$ abolished σ^B activity for cells overexpressing *rsbT* (**Figure 3C**), and in biochemical assays RsbT stimulation of $RsbU^{R91E}$ phosphatase activity was abolished (**Figure 3D**). Finally, we introduced a potentially compensatory charge switch at position D92 of RsbT ($RsbT^{D92K}$) (**Figure 3C**). Expression of $rsbT^{D92K}$ partially restored σ^B activity to $rsbU^{R91E}$ expressing cells, consistent with direct interaction between these residues (**Figure 3C**). Together, these results suggest that contacts between RsbT and the linker of RsbU are responsible for phosphatase activation.

The RsbU linker is flexible in the absence of RsbT

We considered two models for why RsbU is inactive in the absence of RsbT. One possibility is that inactive RsbU resembles the dimeric structure predicted by AlphaFold2 and that RsbT induces a subtle conformational change, for example changing the registry or pitch of the crossing linker helices. A second possibility is that inactive RsbU is dimerized by the N-terminal domains but that the linkers of inactive RsbU are flexible and that the phosphatase domains only interact with each other when RsbT orders the linkers into a crossing conformation. To distinguish between these two models, we performed small angle X-ray scattering coupled to size exclusion chromatography with multi-angle light scattering (SEC-MALS-SAXS) to assess the shape and flexibility of RsbU dimers in solution (Table 1 and **Figure 4 – Figure Supplement 1** -**2** S4A). RsbU eluted as a single peak from the size exclusion column with an average molecular weight of 77 kDa

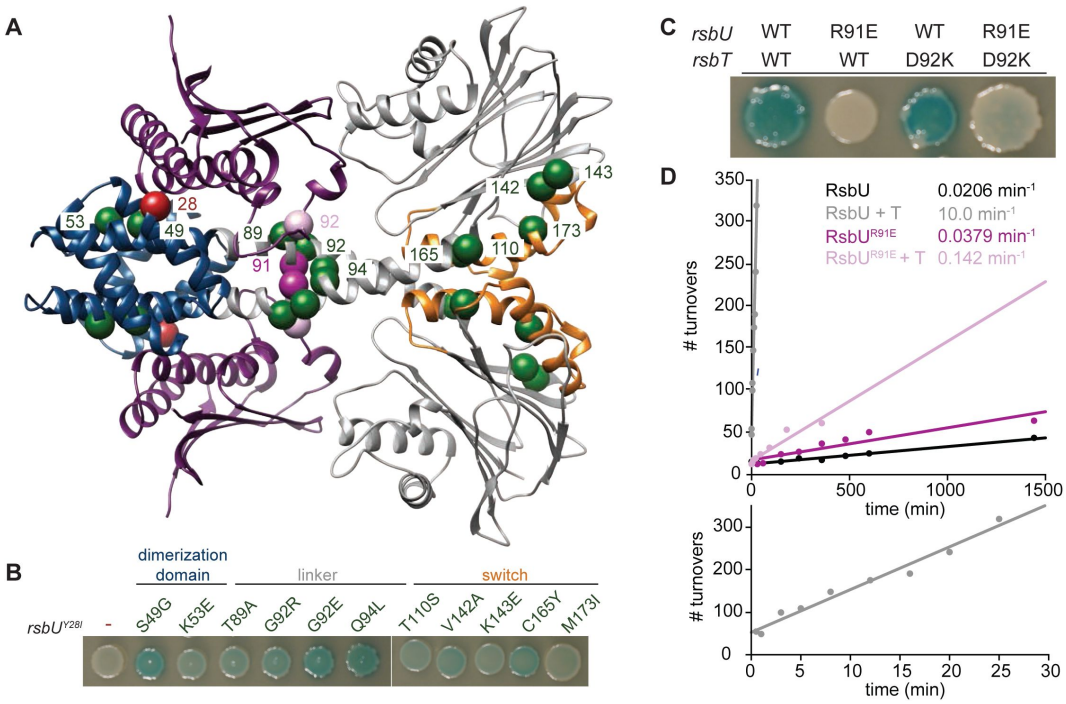

Figure 3

RsbT has a hybrid interface with RsbU N-terminal dimerization domain and linker

A An AlphaFold2 model of a heterotetrameric 2RsbT/2RsbU complex is shown in ribbon representation. RsbT (purple) binds with an interface that spans the N-terminal domains (blue) and α-helical linkers (grey) of both RsbU protomers. The PPM phosphatase domains are colored grey and the regulatory switch elements (α1 and α2) are colored orange. The Cα positions of RsbU^{Y28} (red), rsbU^{Y28I} suppressor substitutions (green), RsbU^{R91} (dark pink), and RsbT^{D92} (pink) are shown as spheres with the residue numbers indicated. **B** Strains with a σ^B LacZ reporter were plated on IPTG/X-gal plates to induce expression of plasmid borne *rsbT* and *rsbU^{Y28I}* and visualize σ^B activity (indicated by blue pigmentation after 24 hours of growth at 37°C). Additional amino acid substitutions in the *rsbU* gene are indicated above the spots, with the region where they are located in the RsbU structure specified. **C** Strains with indicated changes to the RsbT and RsbU amino acid sequence were plated as in B and plates were imaged after 36 hours of growth at 37°C. **D** R91E does not decrease the basal phosphatase activity of RsbU. Plots show dephosphorylation of RsbV-P (25 μM) by RsbU (black) and RsbU^{R91E} (pink) (0.5μM) in the presence of 10 mM $MnCl^2$ and the presence or absence of 10 μM RsbT (light colors). Linear fits of the data are shown, with the slopes indicating the observed rates (kobs): RsbU 0.0206 ± 0.00124 min^{-1}, RsbU + RsbT 10.0 ± 0.628 min^{-1}, RsbU^{R91E} is 0.0379 ± 0.00543 min^{-1}, RsbU^{R91E} + RsbT 0.142 ± 0.0161 min^{-1}. The lower plot is RsbU in the presence of RsbT to thirty minutes.

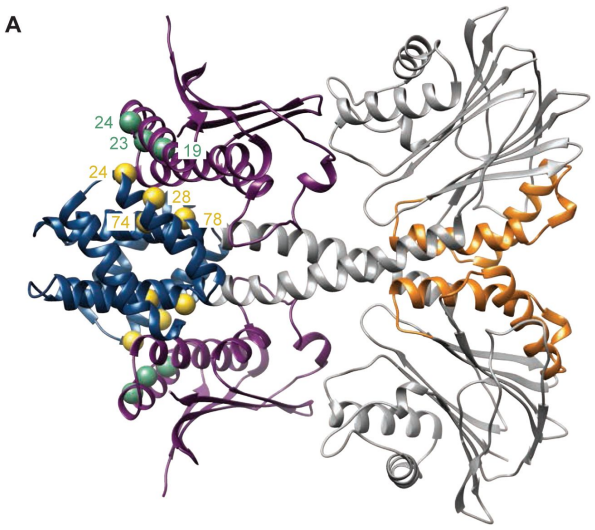

Figure 3 - Supplemental Figure 1

RsbT binds to the linker

A Interface of RsbT and N-terminal domain of RsbU. A ribbon representation is shown of the AlphaFold2 model of the heterote-trameric 2RsbT/2RsbU complex with RsbU N-terminal dimerization domain colored blue, the switch element of the PPM domain (α1 and α2) colored orange, and RsbT colored purple. The Cα of positions of amino acids implicated in the binding interface of RsbT and RsbU N-terminal dimerization domain (Hardwick et al. 2007) are represented on the AlphaFold2 structure as yellow spheres (RsbU) and green spheres (RsbT) with the residue numbers.

(calculated dimeric molecular weight 77.3 kDa) determined by multi-angle light scattering (MALS) (**Figure 4 – Figure Supplement 1**). However, our sample had a minor contaminant of heterodimeric complexes of RsbU in which one monomer is C-terminally truncated that could influence the SAXS analysis (**Figure 4 – Figure Supplement 1**). We therefore deconvoluted the SAXS profiles using evolving factor analysis (EFA) in RAW to isolate scattering profiles from the individual components (Hopkins et al. 2017; Meisburger et al. 2016) (**Figure 4 – Figure Supplement 2**).The EFA deconvolution identified a major component (MW 75.6 kDa calculated from V_c method), which eluted earlier than a smaller component (MW 48.8 kDa calculated from V_c method) (Table 1 Guinier fits, and **Figure 4 – Figure Supplement 2**). We conclude that the larger component is a RsbU dimer, while the smaller fragment is likely a heterodimeric complex of RsbU and the C-terminal truncation product of RsbU (**Figure 4 – Figure Supplement 1**).

Indicative of significant deviation between the RsbU structure in solution to the AlphaFold2 model, the scattering intensity profile (I(q) vs. q) was a poor fit (χ^2 12.53) to a profile calculated from the AlphaFold2 model of an RsbU dimer using FoXS (Schneidman-Duhovny et al. 2016; Schneidman-Duhovny et al. 2013) (**Figure 4A**). We therefore assessed the SAXS data for the RsbU dimer for features that report on flexibility (Kikhney & Svergun 2015). First, the scattering intensity data lacked distinct features caused by the multi-domain structure of RsbU from the AlphaFold2 model (**Figure 4A**). This can be visualized more readily from a dimensionless Kratky plot, which is bell-shaped and peaks above 1.3, indicating that the RsbU dimer is non-globular (**Figure 4B**). Additionally, the data do not show the two peaks from the FoXS computed model of the AlphaFold2 dimer that reflect the extended two domain structure (Kikhney & Svergun 2015; Receveur-Bréchot & Durand 2012) (**Figure 4 – Figure Supplement 2**). The scattering data had several additional characteristic features indicating flexibility: the P(r) plot is smooth and has an extended tail (Cordeiro et al. 2017; Kikhney & Svergun 2015; Receveur-Bréchot & Durand 2012) (**Figure 4C**), R_g and I(0) calculated from P(r) are larger than when calculated from Guinier fits (Cordeiro et al. 2017; Kikhney & Svergun 2015; Receveur-Bréchot & Durand 2012) (Table 1), molecular weight calculated using the MoW2 modified Porod volume method is an overestimate (Rambo & Tainer 2011) (Table 1), and the R_g (39.05 ± 0.16 Å) was larger than the R_g of the AlphaFold2 dimer model (34.05 Å). Prompted by this evidence of flexibility, we performed multi-state modelling using MultiFoXS (Schneidman-Duhovny et al. 2016), which incorporates flexibility and heterogeneity. MultiFoXS produced a two-state solution with χ^2 of 1.2 (as compared to the one-state model with χ^2 of 12.5) and low residuals across the entire range of data (**Figure 4D**, **Figure 4 – Figure Supplement 2**). We allowed flexibility for the linker residues 82-96 while keeping the N-terminal domain dimerized because a stable dimer of the N-terminal domain is observed in solution, was present in a previous X-ray crystal structure of C-terminally truncated RsbU{Delumeau:2004ep}, and C-terminally truncated RsbU coelutes as a heterodimer with the full-length protein (**Figure 4 – Figure Supplement 1**). Importantly, the precise region of allowed linker flexibility does not have a substantial impact on the MultiFoXS fit (**Figure 4 – Figure Supplement 3**), but constraining the C-terminal phosphatase domain dimer does not yield a good fit to the data (χ^2 of 5.4) (**Figure 4 – Figure Supplement 3**). The structural models predicted by MultiFoXS depict a dimerized N-terminal domain with flexible linkers and PPM domains that do not make contact. Notably, this approach also would include models in which both domains remain dimerized, suggesting that such models are not the best fit of the data. The two conformations that were selected as the best fit to the scattering data by MultiFoXS also have very different R_g values, (34.91 Å (71%) and 45.69 Å (29%)), indicating RsbU samples a range of conformational space that includes a more compact state(s) consistent with the AlphaFold2 model and a significantly extended state(s), emphasizing that the linker is highly flexible. Together, we conclude that the RsbU linker appears to be flexible in the absence of RsbT (**Figure 4G**).

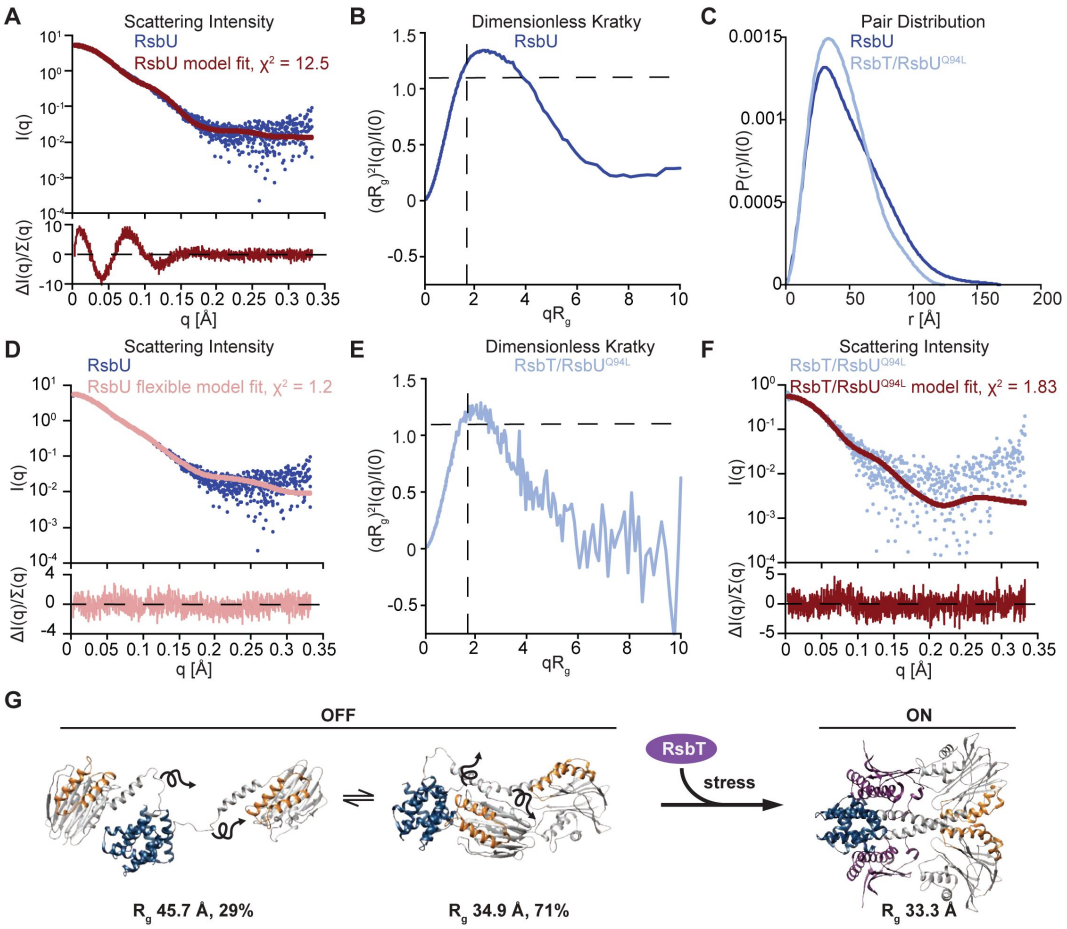

Figure 4

RsbU linker is flexible in the absence of RsbT, and is rigidified by RsbT binding.

A I(q) versus q plot of the dimer component of SAXS scattering data from RsbU (blue) overlaid with a FoXS generated profile fit of the AlphaFold2 RsbU dimer structure (red). The upper plot shows I(q) versus q on log-linear axes while the lower plot shows the uncertainty normalized residuals of the fit ((experimental-computed)/error), χ2 of 12.53. The AlphaFold2 model used for the fit is shown inset. **B** Dimensionless Kratky plot of SAXS scattering data from the dimer component of RsbU experimental data (blue). The experimental profile was logarithmically binned to reduce noise at high qR_g. **C** Normalized P(r) plot from the RsbU dimer (blue) and heterotetrameric RsbT/RsbU^{Q94L} complex (light blue) is shown. **D** I(q) versus q plot of the dimer component of SAXS scattering data from RsbU (blue) is shown overlaid with a MultiFoXS generated two-state profile fit with flexibility allowed for residues 82-96 (pink). The lower plot shows the uncertainty normalized residuals of the fit ((experimental-computed)/error), χ^2 of 1.2. **E** Dimensionless Kratky plot of the heterotetrameric component of RsbT/RsbU^{Q94L} complex is shown binned logarithmically to reduce noise at high qR_g values. **F** I(q) versus q plot of the heterotetrameric component of SAXS scattering data from RsbT/RsbU^{Q94L} complex (blue) overlaid with a FoXS generated profile fit of the AlphaFold2 RsbT/RsbU heterotetramer structure (red). The upper plot show I(q) versus q on a log-linear axes while the lower plot shows the uncertainty normalized residuals of the fits ((experimental-computed)/error), χ2 of 1.83.**G** Schematic of the conformational change of RsbU upon RsbT binding. The two best fit flexible models of RsbU generated from MultiFoXS in panel B are shown with the calculated R_g and percentage of each model used in the fit indicated. These two models are shown in exchange with arrows to indicate flexibility. The AlphaFold2 model of 2RsbU/2RsbT heterotetramer used for the FoXS fit in E is shown with the calculated R_g indicated.

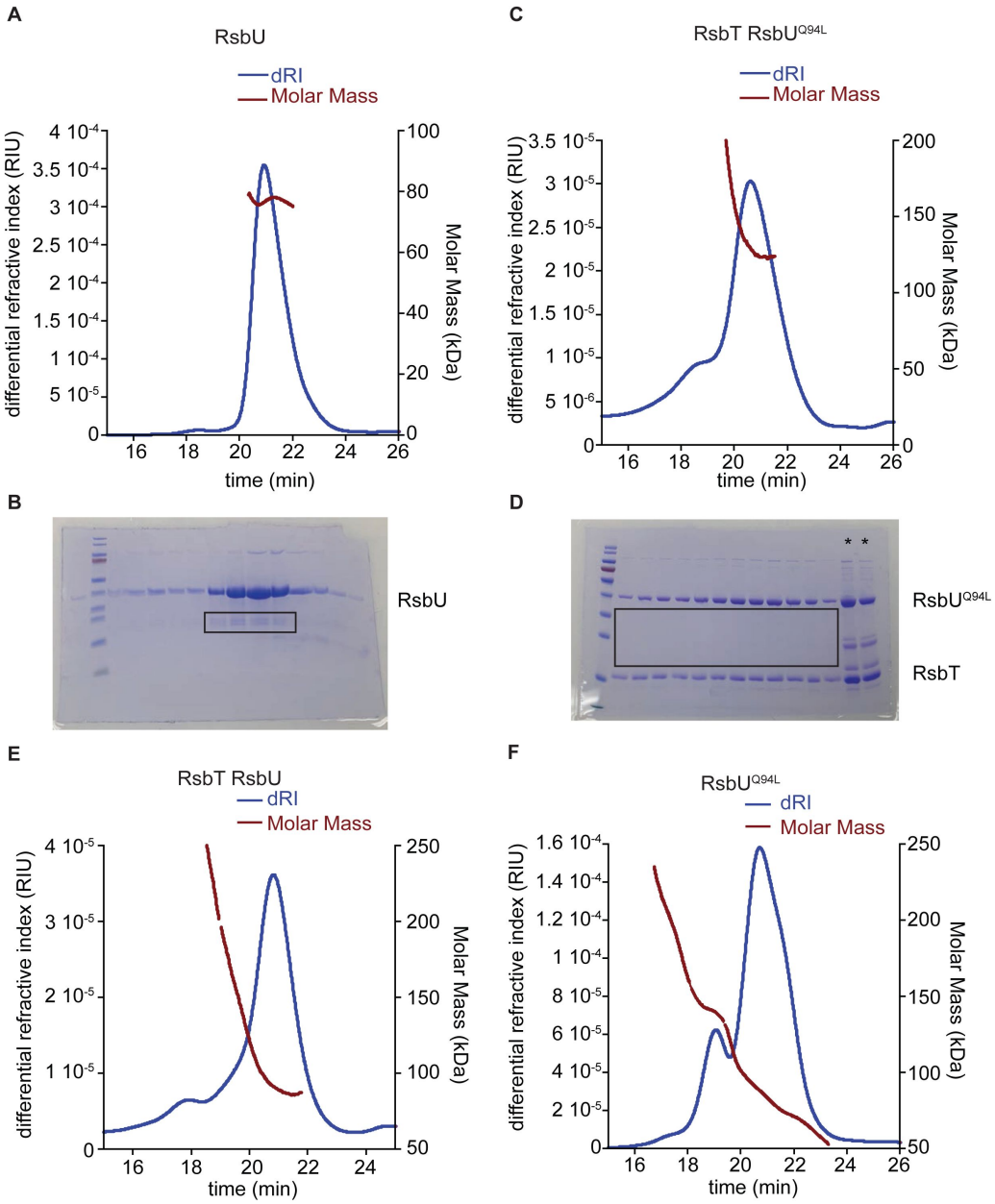

Figure 4 - Supplemental Figure 1

MALS estimate of molecular weight of RsbU dimer, RsbT/RsbUQ94L complex, RsbT/RsbU complex, and RsbUQ94L

A Plot of inline SEC-MALS analysis of RsbU with measured differential refractive index (blue, left axis) and the molecular weight calculated from MALS (red, right axis). **B** Denaturing SDS-PAGE gel of successive fractions from the equivalent range of the elution as shown in A from preparative size exclusion chromatography of the sample of RsbU used for SEC-MALS-SAXS. Black box denotes the C-terminal truncation product present in each lane of the main peak. **C** Plots from inline SEC-MALS analysis of RsbT/RsbU^{Q94L} complex with measured differential refractive index (blue, left axis) and the molecular weight calculated from MALS (red, right axis). **D** Denaturing SDS-PAGE gel of successive fractions from the equivalent range of the elution of RsbT/U^{Q94L} as shown in C from preparative size exclusion chromatography of the sample used for SEC-MALS-SAXS. Black box denotes lack of C-terminal truncation product during co-expression and purification of RsbT/RsbU^{Q94L} complex. * Denotes load samples on gel. **E** Plots from inline SEC-MALS analysis of RsbT/U complex with measured differential refractive index (blue, left axis) and the molecular weight calculated from MALS (red, right axis). **F** Plot inline SEC-MALS analysis of RsbU^{Q94L} with measured differential refractive index (blue, left axis) and the molecular weight calculated from MALS (red, right axis).

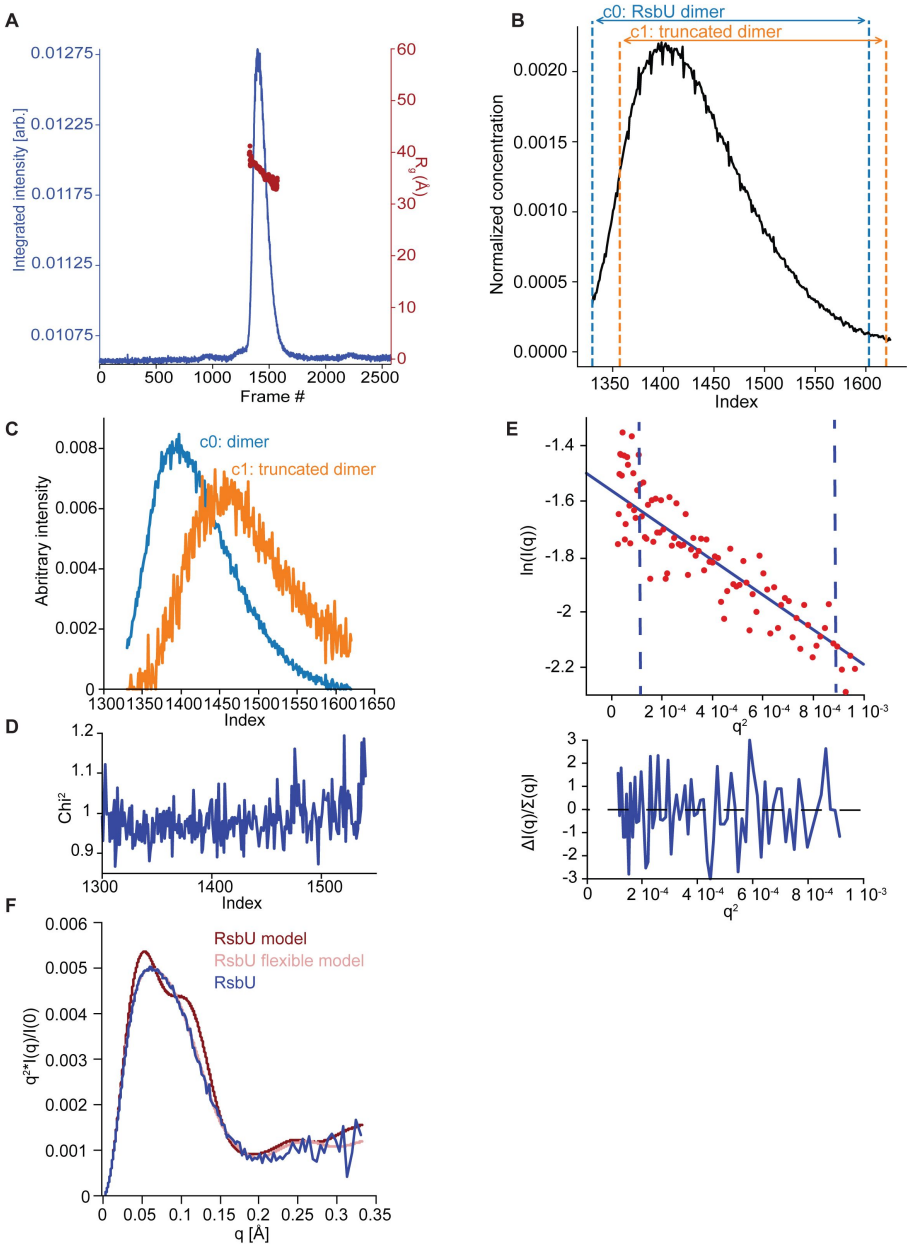

Figure 4 - Supplemental Figure 2

EFA deconvolution and Guinier analysis of RsbU dimer SAXS profiles

A SAXS data summary for RsbU. Series intensity (blue, left axis) versus frames, and R_g versus frame (red, right axis) are plotted. **B** The selected intensity range for EFA (black) (frame index 1330-1620), and the individual component ranges for deconvolution; blue denotes the range of frames where the scattering component we assigned as the c0, RsbU dimer, was detected (frame index 1330-1603) and orange denotes the range of frames where the scattering component that is c1, presumably from a RsbU heterodimer containing a c-terminal truncation product dimer (frame index 1357-1620). **C** Area normalized concentration profiles for the c0, RsbU dimer component (blue) and c1, RsbU heterodimer containing c-terminal truncation product dimer (orange). **D** Mean χ2 values for the fit of the EFA deconvolution to the original scattering data. **E** Guinier fit for RsbU dimer component on the upper plot and uncertainty normalized residuals of the fit on the lower plot. The scattering data for the dimer component (red) is fit to the Guinier approximation (blue). The blue dashed lines are the q_{min} and q_{max} at values 0.00356 Å-1 and 0.0234 Å-1, respectively. **F** Kratky plot of SAXS scattering data from the dimer component of RsbU experimental data (blue) overlaid with the profile computed by FoXS based on the AlphaFold2 model of an RsbU dimer (red) and the profile of the flexible model computed by MultiFoXS (pink). The experimental profile was logarithmically binned to reduce noise at high q.

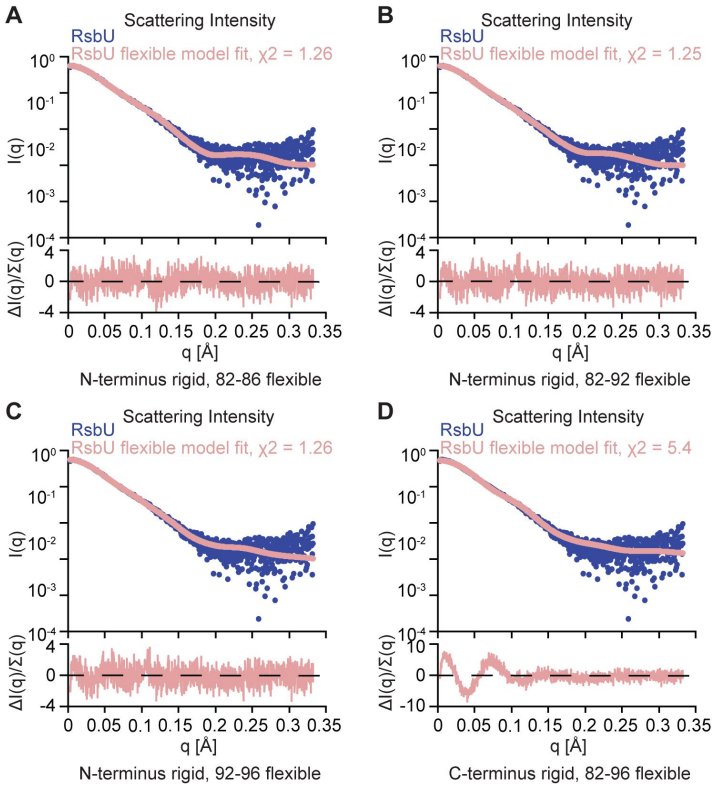

Figure 4 - Supplemental Figure 3

Varying constraints and flexibility of RsbU model

A I(q) versus q plot of the dimer component of SAXS scattering data from RsbU (blue) overlaid with a MultiFoXS generated two-state profile fit with flexibility allowed for residues 82-86 (pink). The upper plot shows I(q) versus q on log-linear axes while the lower plot shows the uncertainty normalized residuals of the fit ((experimental-computed)/error), χ^2 of 1.26. **B** I(q) versus q plot of the dimer component of SAXS scattering data from RsbU (blue) overlaid with a MultiFoXS generated two-state profile fit with flexibility allowed for residues 82-92 (pink). The upper plot shows I(q) versus q on log-linear axes while the lower plot shows the uncertainty normalized residuals of the fit ((experimental-computed)/error), χ^2 of 1.25. **C** I(q) versus q plot of the dimer component of SAXS scattering data from RsbU (blue) overlaid with a MultiFoXS generated two-state profile fit with flexibility allowed for residues 92-99 (pink). The upper plot shows I(q) versus q on log-linear axes while the lower plot shows the uncertainty normalized residuals of the fit ((experimental-computed)/error), χ^2 of 1.26. **D** I(q) versus q plot of the dimer component of SAXS scattering data from RsbU (blue) overlaid with a MultiFoXS generated two-state profile fit with flexibility allowed for residues 82-96 (pink) and the C-terminal domains constrained. The upper plot shows I(q) versus q on log-linear axes while the lower plot shows the uncertainty normalized residuals of the fit ((experimental-computed)/error), χ^2 of 5.4.

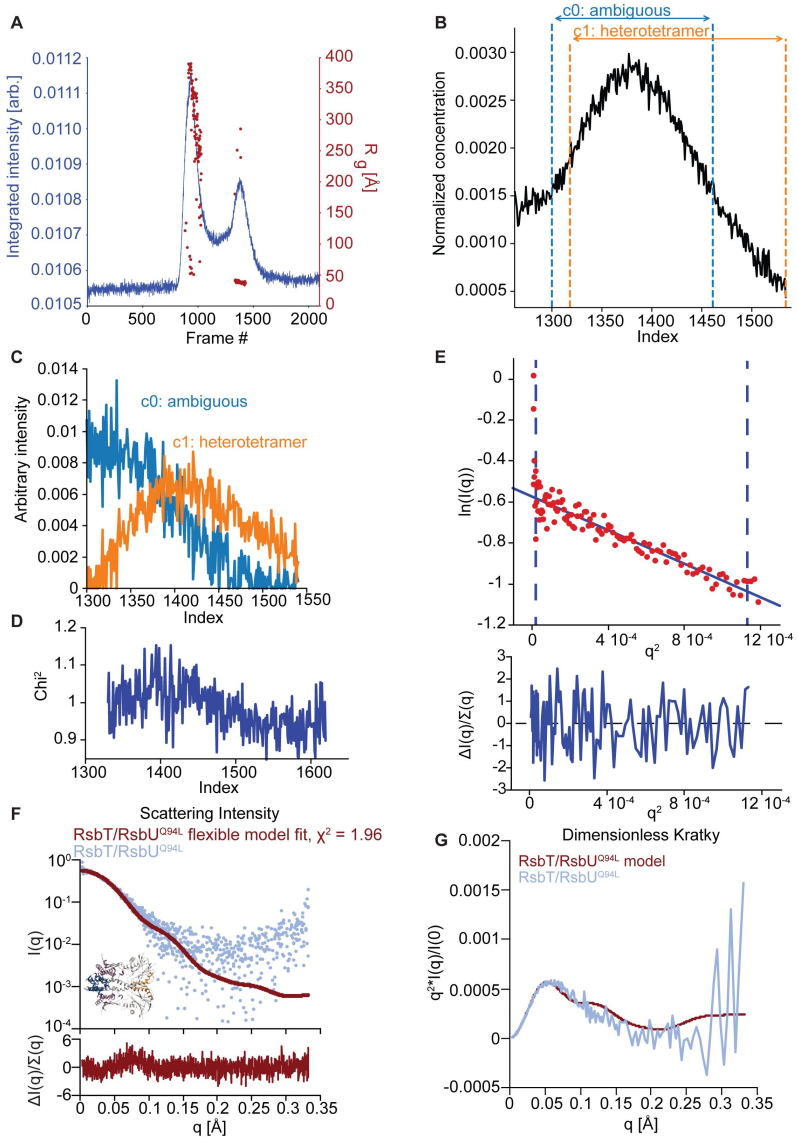

Figure 4 - Supplemental Figure 4

EFA deconvolution and Guinier analysis of RsbT/RsbU^{Q94L} SAXS profiles

A SAXS data summary for RsbT/RsbU^{Q94L}. Series intensity (blue, left axis) versus frames, and R_g versus frame (red, right axis) are plotted. **B** The selected intensity range for EFA (black) (frame index 1300-1540), and the individual component ranges for deconvolution; blue denotes the range of frames where the scattering component we assigned as c0, ambiguous component, was detected (1300-1461) and orange denotes the range of frames where the scattering component we assigned as c1, the 2RsbT/2RsbU^{Q94L} heterotetrametric complex, was detected (1318-1540). **C** Area normalized concentration profiles for 2RsbT/2Rs-bU^{Q94L} heterotetrameric complex (orange) and ambiguous component (blue). D Mean χ^2 values for the EFA deconvolution fit to the original scattering data. **E** Guinier fit for 2RsbT/2RsbU^{Q94L} heterotetrameric complex component on the upper plot and uncertainty normalized residuals of the fit on the lower plot. The scattering data for the dimer component (red) is fit to the Guinier approximation (blue). The blue dashed lines are the q_{min} and q_{max} at values 0.0033 Å^{-1} and 0.0336 Å^{-1}, respectively. **F** I(q) versus q plot of the heterotetrameric complex component of SAXS scattering data from 2RsbT/2RsbU (blue) overlaid with a MultiFoXS generated two-state profile fit with flexibility allowed for residues 82-96 (red). The upper plot shows I(q) versus q on log-linear axes while the lower plot shows the uncertainty normalized residuals of the fit ((experimental-computed)/error), χ^2 of 1.96. The one-state flexible model is shown with a RMSD to the AlphaFold2 prediction of 2RsbT/2RsbU of 1.36 Å. **G** Kratky plot of SAXS scattering data from the heterotetrameric component of 2RsbT/2RsbU experimental data (blue) overlaid with the profile computed by FoXS based on the AlphaFold2 model of an RsbT/RsbU heterotetramer (red). The experimental profile was logarithmically binned to reduce noise at high q.

RsbT rigidifies and compacts the RsbU dimer

To test the hypothesis that RsbT rigidifies the linker to produce an active RsbU dimer, we attempted SEC-MALS-SAXS analysis of the RsbT/U complex. RsbT/U eluted with molecular weight (determined by MALS) of 88 kDa compared to 105 kDa for a 2RsbT/2RsbU heterotetramer (**Figure 4 – Figure Supplement 1**), suggesting that the RsbT/U complex had largely disassembled on the column. We therefore performed SEC-MALS-SAXS on the RsbT/RsbU^{Q94L} complex, which has a higher affinity (**Figure 2A**, **Figure 4 - Figure Supplement 4**). The RsbT/U^{Q94L} complex eluted as a major peak with a higher molecular weight shoulder (**Figure 4 - Figure Supplement 1**, **4**) (also visible when we ran RsbU^{Q94L} alone. **Figure 4 – Figure Supplement 1**), with the average molecular weight of the main peak (determined by MALS) of 125 kDa (**Figure 4 – Figure Supplement 1**). This is larger than the predicted molecular weight of a heterotetrameric 2RsbT/2RsbU^{Q94L} complex (105 kDa), suggesting that some higher order complexes form. EFA deconvolution (Meisburger et al. 2016) identifies two components. The first deconvolved component had a SAXS determined molecular weight of 164 kDa, while the second had a SAXS molecular weight of 103 kDa, consistent with a 2RsbT/2RsbU complex (105 kDa). Together with the fact that RsbT co-elutes with RsbU^{Q94L} throughout the entire peak (**Figure 4 – Figure Supplement 1**) and the MALS molecular weight, we assess that this second component is an 2RsbT/2RsbU hetero-tetramer. The identity of the higher molecular weight component of the scattering data is ambiguous, but could represent a larger assembly of RsbT/RsbU^{Q94L} or multimers of RsbU^{Q94L} that were observed when RsbU^{Q94L} was analyzed alone (**Figure 4 – Figure Supplement 1**). Several lines of evidence demonstrate that the 2RsbT/2RsbU^{Q94L} complex lacks the flexibility of the 2RsbU complex. First, the R_g from the Guiner fit (35.06 ± 0.43 Å) matches well with the model computed from the AlphaFold2 prediction of the heterotetrameric complex of 2RsbT/2RsbU using FoXS (33.68 Å) and is smaller than the R_g we observed for the RsbU dimer (39.05 ± 0.16 Å). Second, the features of the scattering data that suggested flexibility for RsbU dimers all suggest that the RsbT/RsbU complex is more rigid (the quality of the FoXS fit, a lower peak of the dimensionless Kratky plot, and a shorter tail of the P(r) plot) (Cordeiro et al. 2017; Kikhney & Svergun 2015; Receveur-Bréchot & Durand 2012) (**Figure 4C**,**4E**-**4F**, **Figure 4 – Figure Supplement 4**). Third, fitting the scattering profile (I(q) vs. q) to the AlphaFold2 model yielded a χ^2 of 1.83 without requirement for flexibility (**Figure 4E**). As expected, based on the lack of evidence of flexibility in the scattering profile and P(r) function, the model is not improved by the use of multi-state modeling by MultiFoXS, which was run as a control (Schneidman-Duhovny et al. 2016) (**Figure 4 - Figure Supplement 4**). Together, these data support the validity of the AlphaFold2 model of the heterotetrameric 2RsbT/2RsbU complex, and additionally suggest that RsbT rigidifies the otherwise flexible linker of RsbU to dimerize the phosphatase domains (**Figure 4G**). Together with our biochemical data linking RsbU linker conformation to RsbT binding, metal cofactor interaction, and phosphatase activity, this provides a comprehensive model for how RsbU is activated (**Figure 4G**).

Regulated dimerization is an evolutionarily adaptable mechanism to control bacterial phosphatases

B. subtilis has a second GSR-initiating PPM phosphatase, RsbP, that has an N-terminal PAS domain and dephosphorylates RsbV to activate σ^B in response to energy stress. Our AlphaFold2 prediction of an RsbP dimer shows an extended alpha-helical linker connecting dimeric PAS domains and phosphatase domains. Like RsbU, the interface between the dimerized phosphatase domains is predicted to be mediated by α1 and α2 of the phosphatase domain. We found that previously identified constitutively activating mutations in RsbP (Brody et al. 2009) map to similar positions as the gain-of-function mutations we identified here for RsbU in their respective predicted structures, namely the interface between α1 and α2 of the phosphatase domains and the linker. RsbP is activated by a partner-protein, RsbQ, that has analogous function to RsbT for RsbU. An AlphaFold2 prediction of the heterotetrameric 2RsbP/2RsbQ complex places the two molecules

of RsbQ in a hybrid interface between the PAS domains and linkers, similar to how RsbT contacts RsbU. These predictions suggest a testable hypothesis that RsbP is controlled through an activation mechanism similar to that of RsbU (**Figure 5A**).

To further probe the generality of the linker-mediated phosphatase dimer we observe for RsbU, we generated AlphaFold2 predictions for dimers of other documented GSR initiating phosphatases (*C. difficile* RsbZ (N-terminal tandem GAF domains) (**Fig. 5B**), *S. coelicolor* OsaC (N-terminal GAF and PAS domains), and *M. tuberculosis* Rv1364c (N-terminal PAS domain, C-terminally fused to an anti-σ factor domain and an anti-anti-σ factor domain)), as well as from examples of common domain architectures of PPM phosphatases selected from InterPro (response receiver (*Streptomyces coelicolor*, MY40396.1), GAF (*Rhodococcus aetherivorans*, WP_029544106.1), and HAMP (*Synechocystis sp.*, WP_010874143.1) domains) (**Figure 5 – Figure Supplement 1**). In each case AlphaFold2 produced high-confidence predictions of phosphatase domains dimerized through a shared α0, α1, α2 interface, connected to dimeric N-terminal domains by crossing α-helical linkers (**Figure 1 – Figure Supplement 1**-**2**, **Figure 5 – Figure Supplement 1**). Consistent with a model in which the stability of the linker plays a conserved regulatory role, the AlphaFold2 models for many of the predicted structures have unfavorable polar residues buried in the coiled-coil interface (positions *a* and *d*, for which non-polar residues are most favorable) (**Figure 5 – Figure Supplement 2**). From this analysis, we speculate that linker-mediated phosphatase domain dimerization is an evolutionarily conserved, adaptable mechanism to control PPM phosphatase activity. This mechanistic/structural congruence provides a framework for how distantly related phosphatases can be regulated to control diverse biological processes in bacteria (**Figure 5E**).

Discussion

Since the ground-breaking discovery of σ^B, the first conditionally-activated cellular transcription factor to be identified, forty-five years ago (Haldenwang & Losick 1979), a persistent unanswered question has been how σ^B is turned on. Here, our findings reveal how RsbU is activated as a phosphatase in the decisive step of σ^B activation. Below, we describe how this mechanism is broadly applicable to other bacterial signaling pathways.

RsbT activates RsbU through a conserved phosphatase dimer

Using unbiased genetic screens, biochemical reconstitution, biophysical approaches, and structural prediction, we have discovered that RsbT activates RsbU by rigidifying an otherwise flexible linker region to allosterically activate RsbU as a phosphatase. Our structural prediction, supported by our genetic and structural data suggest that RsbU linkers assume a crossed α-helical conformation that dimerizes the phosphatase domains (**Figure 4G**). This dimerization activates RsbU through a conserved switch element at the dimer interface, decreasing the K_M for metal cofactor and increasing the catalytic rate. Our structural predictions suggest that this is a widespread mechanism to regulate the activity of bacterial protein serine/threonine phosphatases. While RsbU activation is controlled by a flexible-to-rigid transformation of the linker, it is possible that other conformational changes of the linker could be alter the PPM dimer to control phosphatase activity through the conserved switch element.

A general mechanism for general stress response activation

E. coli and *B. subtilis* are the most extensively studied models for GSR activation (Battesti et al. 2011; Hecker et al. 2007). However, key mechanistic features of the activation mechanisms differ between the two systems. The *E. coli* GSR is initiated by stabilizing the alternative sigma factor σ^S (RpoS) against degradation by ClpXP (**Figure 5C**). Under non-stressed conditions, degradation of σ^S is mediated by the adapter protein, RssB, which is inhibited by anti-adaptors

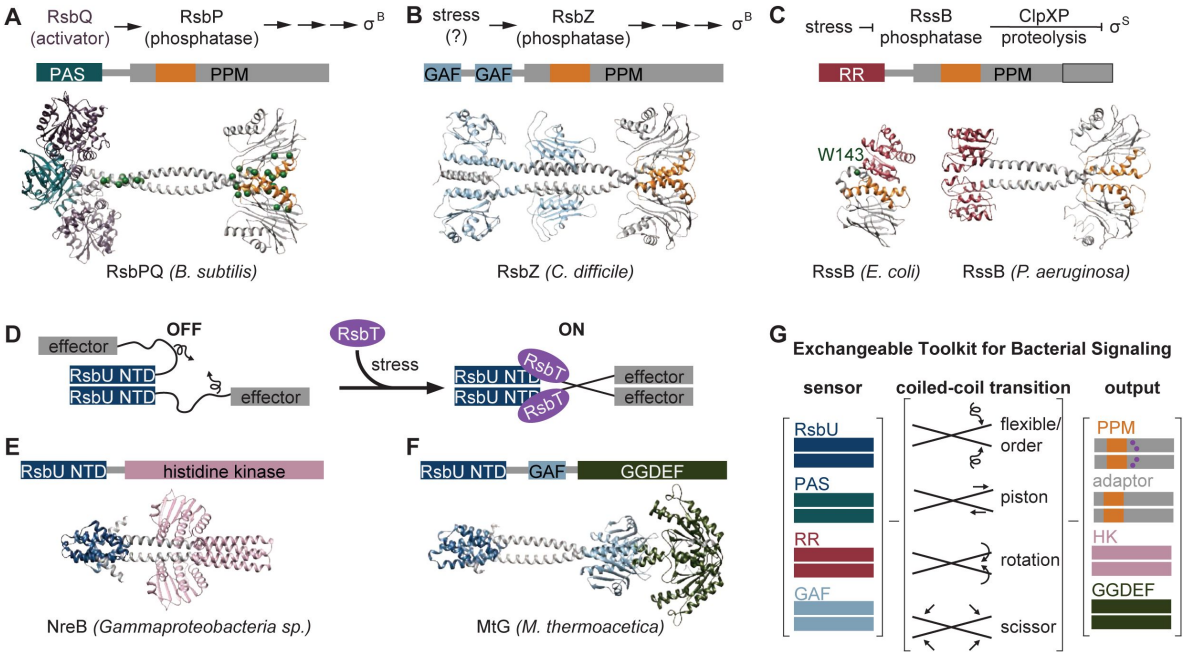

Figure 5

An exchangeable toolkit for bacterial signal transduction

A An AlphaFold2 model of the *B. subtilis* energy stress phosphatase RsbP is shown bound to its activating α/β-hydrolase protein RsbQ (purple) with a schematic of the σB activation pathway shown above. RsbP has an N-terminal PAS domain (turquoise) that is connected to the PPM phosphatase domain by a predicted coiled coil linker. The Cα positions of bypass suppressor mutations that render RsbP active in the absence of RsbQ(Brody et al. 2009) are shown as green spheres. The switch element of the PPM phosphatase domain (α1 and α2) is colored orange. **B** An AlphaFold2 model of the *C. difficile* GSR phosphatase RsbZ is shown with a schematic of the σ^B activation pathway shown above. RsbZ has tandem N-terminal GAF domains (blue) that connect to the PPM phosphatase domain by a predicted coiled coil linker. The switch element of the PPM phosphatase domain (α1 and α2) is colored orange. **C** Experimental structures of the GSR initiating adaptor protein RssB from *E. coli* (left, 8T85) and *P. aeruginosa* (right, 3F7A) are shown with a schematic of the σ^S activation pathway shown above. The Cα positions of a bypass suppressor mutation (W143R) that renders RssB insensitive to anti-adapter proteins is shown as a green sphere. The switch element of the PPM phosphatase domain (α1 and α2) is colored orange. The black outline shows the portion of hte PPM phosphatase domain that is missing in the *E. coli* RssB adaptor protein, which lacks phosphatase activity. **D** A cartoon schematic of activation by RsbT of proteins with RsbU NTD through ordering of a flexible linker. The protein is depicted with dimerized RsbU N-terminal dimerization domains (blue) with flexible linkers (black) that extend into two effector domains (grey). During stress conditions, RsbT (purple) activates the protein through binding to hte N-terminal dimerization domains and linkers, rigidifying the linkers to dimerize the effector domains. **E** An AlphaFold2 model of a dimer of the histidine kinase NreB from a *Gammaproteobacteria* species (MBI3545564.1) is shown with the RsbU N-terminal domain colored blue and the histidine kinase domain colored pink. **F** An AlphaFold2 model of a dimer of the GGDEF diguanylate cyclase MtG from *M. thermoacetica* (WP_011392981.1) is shown with RsbU N-terminal domain colored blue, GAF domain colored lite blue, and GGDEF domain colored green. **G** Schematic illustrating how various sensor domains (RsbU N-terminal dimerization domain, PAS, response receiver (RR), and GAF) can control various output activities (serine/threonine phosphatase (PPM), histidine kinase (HK), protease adaptor, and diguanylate cyclase (GGDEF). We hypothesize that the shared regulatory mechanism through a dimeric coiled-coil linker makes these regulatory domains modularly exchangeable across effector domains. Known mechanisms for how allosteric regulation is transmitted through the linker are listed and shown with arrow diagrams.

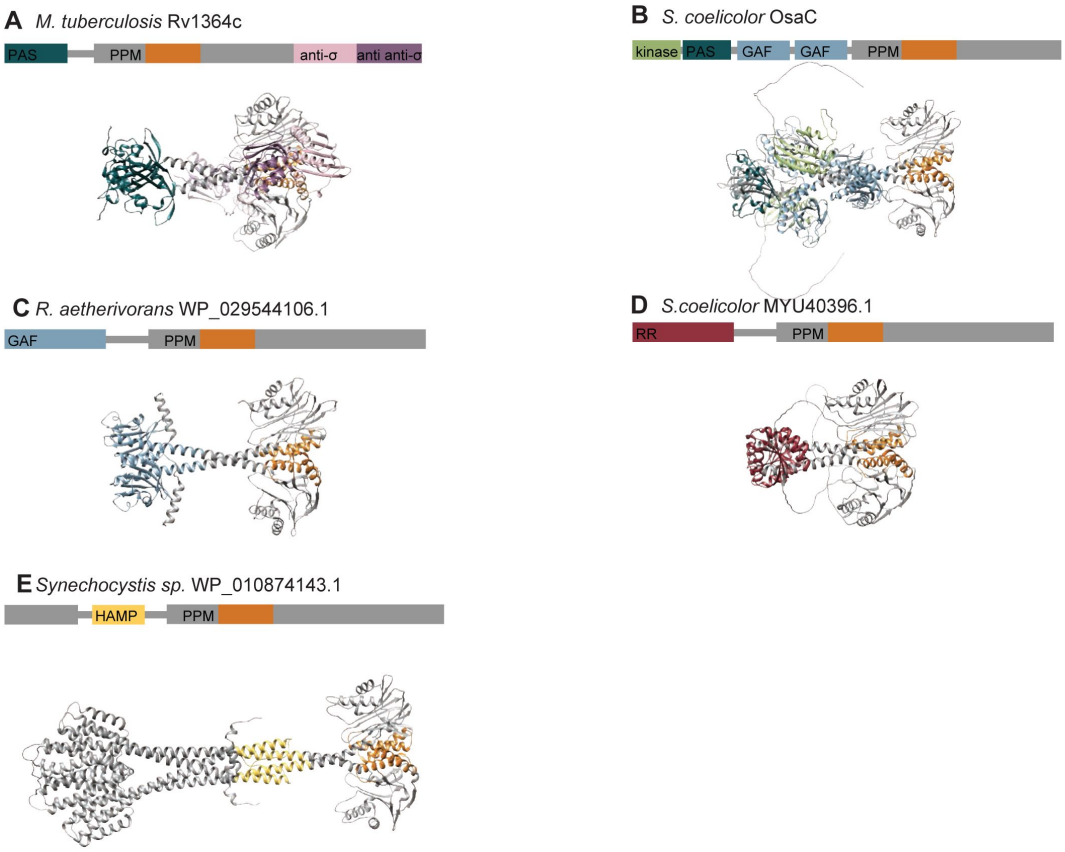

Figure 5 - Supplemental Figure 1

AlphaFold2 predictions of varying signaling PPM phosphatases

A An AlphaFold2 model of the *M. tubercolisis* GSR phosphatase Rv1364c is shown with a N-terminal PAS domain colored turquoise that connects to the PPM phosphatase domain colored grey, an anti-σ domain (related to RsbW) colored pink and an anti-anti-σ domain (related to RsbV) colored purple. The switch element of the PPM phosphatase domain (α1 and α2) is colored orange. **B** An AlphaFold2 model of the *S. coelicolor* OsaC GSR phosphatase is shown with a N-terminal RsbW-like kinase domain colored in green, connected to a PAS domain colored in turquoise, tandem GAF domains colored in blue, and a PPM phosphatase colored in grey. The switch element of the PPM phosphatase domain (α1 and α2) is colored orange. **C** An AlphaFold2 model of a dimer of the phosphatase from *R. aetherivorans* (WP_029544106.1) is shown with the GAF domain colored in blue connected to the PPM phosphatase colored in grey. The switch element of the PPM phosphatase domain (α1 and α2) is colored orange. **D** An AlphaFold2 model of a dimer of the phosphatase from *S. coelicolor* (MYU40396.1) is shown with the response receiver domain colored in red connected to the PPM phosphatase colored in grey. The switch element of the PPM phosphatase domain (α1 and α 2) is colored orange. **E** An AlphaFold2 model of a dimer of the phosphatase from *Synechocystis species* (WP_010874143.1) is shown with the HAMP domain colored in yellow connected to the PPM phosphatase colored in grey. The switch element of the PPM phosphatase domain (α1 and α2) is colored orange. The structure models in all panels are shown aligned by the top PPM domain to highlight the conservation of the PPM dimer in predictions of dimeric phosphatases with diverse regulatory domains.

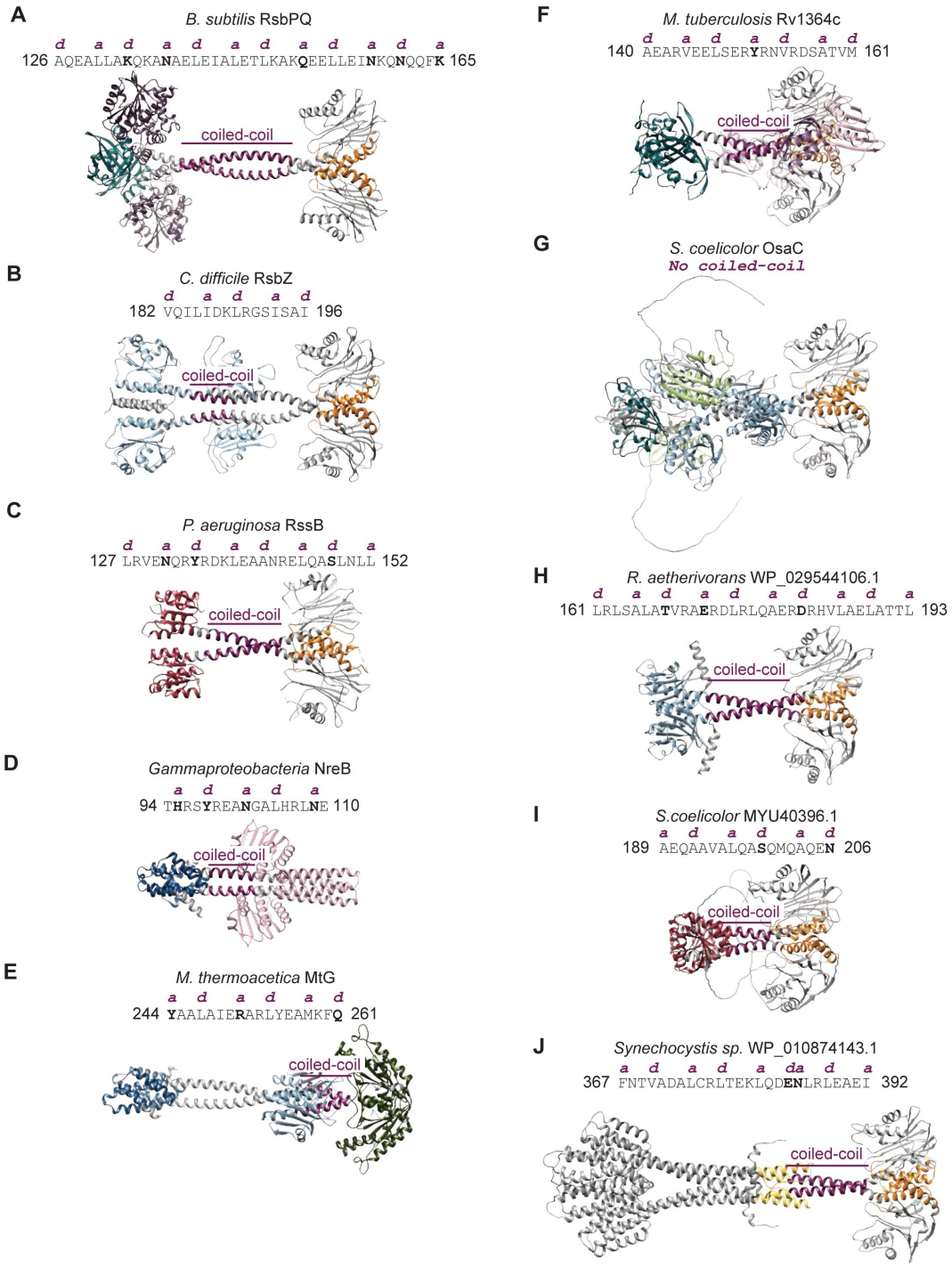

Figure 5 - Figure Supplement 2

Coiled-coil analysis of structures of bacterial signaling enzymes

Models of selected phosphatases are shown: **A**, heterotetramer of RsbPQ from *B. subtilis*; **B**, RsbZ from *C. difficile*; **C**, RssB from *P. aeruginosa* (PDB: 3EQ2); **D**, NreB from *Gammaproteobacteria*; **E**, MtG from *M. thermoacetica*; **F**, Rv1364c from *M. tuberculosis*; **G**, OsaC from *S. coelicolor*; **H**, WP_029544106.1 from *R. aetherivorans*; **I**, MYU40396.1 from *S. coelicolor*; **J**, WP_010874143.1 from *Synechocystis sp.*. Coiled-coil sequences identified by Socket2 are shown above the model with the non-polar positions of a and d shown in pink above the sequence. Polar residues at the a and d positions are in bold. The coiled-coil region on the model is shown in pink, the switch helices of the PPM domains are shown in orange, and the various regulatory domains are shown in the following colors: RsbU NTD (blue), PAS (green), GAF (light blue), response receiver (red), and HAMP (yellow).

(IraD, IraM, and IraP) and stimulated by phosphorylation on its N-terminal response-receiver domain during stress. Historically, the differences between these systems were interpreted to mean that they operate by distinct mechanistic principles. However, RssB contains a C-terminally truncated (and therefore inactive) PPM phosphatase domain, suggesting some aspects of its regulatory mechanism could be shared with RsbU (Battesti et al. 2013).

Our findings reveal that *E. coli* RssB and *B. subtilis* RsbU use three shared regulatory features to control GSR activation through their distinct downstream mechanisms. First, the positioning of analogous flexible linkers controls GSR activation by RssB and RsbU (Brugger, Schwartz, et al. 2023; Brugger, Srirangam, et al. 2023; Dorich et al. 2019). The C-terminal pseudo-phosphatase domain of RssB is joined to its N-terminal σ^S binding response-receiver domain by a predominantly α-helical linker (termed the segmented helical linker, or SHL) of similar length to the linker of RsbU (Dorich et al. 2019). The SHL folds to occlude the σ^S interacting face of the response-receiver domain when bound to anti-adapters, and is remodeled to promote σ^S interaction when the response-receiver domain is phosphorylated (Brugger, Schwartz, et al. 2023; Brugger, Srirangam, et al. 2023; Dorich et al. 2019). Supporting the hypothesis that the SHL is mechanistically related to the RsbU linker, substitution of W143, the homologous residue to Q94 of *B. subtilis* RsbU, blocks regulation by IraD and IraP (Battesti et al. 2013). Second, the interface between the linker and α1 of the phosphatase domain is critical for regulation of both RssB and RsbU (Brugger, Schwartz, et al. 2023; Dorich et al. 2019). W143 packs in a hydrophobic pocket formed with the α1 helix of the pseudo-phosphatase domain of phosphorylated RssB and IraD bound RssB (Brugger, Schwartz, et al. 2023; Dorich et al. 2019). Substitution of residues in α1, including A216 (corresponding to M166 of RsbU), block regulation of RssB by anti-adapters, underscoring the mechanistic similarity (Battesti et al. 2013). Third, conformational change of the switch helices (α1 and α2) of the phosphatase domain is of shared regulatory importance (Battesti et al. 2013). HDX experiments demonstrate that there is decreased exchange of the α1 helix of the pseudo-phosphatase domain of RssB when σ^S is bound, suggesting that the conformational dynamics of this region are reduced by substrate recognition (Brugger, Schwartz, et al. 2023).

These striking mechanistic similarities between RssB from *E. coli* and RsbU from *B. subtilis* suggest that key regulatory features were conserved when an ancestral phosphatase lost enzymatic activity and became a dedicated adapter protein in *E. coli* and related γ-proteobacteria. Interestingly, *P. aeruginosa* has a homologue of RssB/RsbU that functions as an adapter for σ^S degradation, yet has a catalytically active, full length phosphatase domain and resides in an operon with an *rsbV* homologue (*rssC)* (Rodríguez-Martínez et al. 2023). Crystal structures of *P. aeruginosa* RssB revealed that it forms a dimer with crossing linkers and dimerized phosphatase domains with striking similarity to the dimer predicted for RsbU (**Fig. 5C**, S2C). Intriguingly, adapter protein function of *P. aeruginosa* RssB requires RssC (Rodríguez-Martínez et al. 2023), and *E. coli* RssB has been observed to weakly dimerize (Dorich et al. 2019), further supporting a direct mechanistic link between phosphatase regulation and adapter protein function. While not all GSR regulatory mechanisms involve a phosphatase or adapter protein related to RsbU/RssB, these findings suggest that linker-mediated control of a PPM phosphatase is a broadly conserved mechanism for GSR initiation across bacterial phyla.

An exchangeable toolkit for signal transduction

Histidine kinases and GGDEF diguanylate cyclases are the two most prevalent families of bacterial signal transduction proteins. A striking feature of their regulatory mechanisms is that they are often active in dimeric complexes that are allosterically controlled by N-terminal regulatory domains that propagate signals through crossing α-helical linkers (Zschiedrich et al. 2016; Randall et al. 2022; Gourinchas et al. 2017). Our findings that the crossing α-helical linkers are structurally similar (Fig. S2C), and that shared regulatory domains (response receiver, HAMP, and PAS domains) connect phosphatase dimers by a coiled-coil linker (**Figure 5A-C**, **Figure 5 – Figure Supplement 1**) suggests that this shared allosteric regulatory architecture allows

modular exchange of N-terminal domains between PPM phosphatases, histidine kinases, and GGDEF diguanylate cyclases (**Figure 5D**). In support of this, the RsbU N-terminal domain and RsbT were previously shown to control GGDEF diguanylate cyclase activity in *Moorella thermoacetica* (Quin et al. 2012), histidine kinases with RsbU N-terminal domains are found in operons with *rsbT* and stressosome genes in some *Proteobacteria* species (Heinz et al. 2022), and AlphaFold2 prediction of these dimeric complexes reveals coiled-coil linkers to the effector domains (**Figure 5E-F**). Similarly, the PAS/α/β hydrolase module that controls RsbP phosphatase activity in *B. subtilis* is found coupled to histidine kinases and GGDEF diguanylate cyclases across bacterial phyla (Nadezhdin et al. 2011).

While the specific mechanism discovered here for linker control of RsbU activity (flexibility controlled by a binding partner) is distinct from the models for linker control of histidine kinases and GGDEF diguanylate cyclases (piston shift, scissoring, and helical rotation) (Zschiedrich et al. 2016; Randall et al. 2022), the shared dimeric architecture suggests that N-terminal regulatory domains could be modularly exchanged across effector domain families (**Figure 5G**). Allosteric control of PPM switch element conformation could theoretically be achieved by piston shift, scissoring, or helical rotation. Future characterization of PPM phosphatases will be required to determine how widespread linker flexibility is as a regulatory mechanism and how modularly sensory domains can be exchanged across signaling effector families.

Materials and methods

Protein expression and purification

All proteins were expressed in *E. coli* BL21 (DE3) cells grown at 37°C to an OD_{600} of 0.4 and induced at 16°C for 14-18 hours with 1mM isopropyl β-d-1-thiogalactopyranoside (IPTG) unless otherwise specified. Cells were harvested and purified as follows:

RsbU and RsbU variants

Cell pellets were resuspended in lysis buffer with 1 mM phenylmethylsulfonyl fluoride (PMSF) (50 mM K•HEPES, pH 7.5, 100 mM NaCl, 20 mM imidazole, 10% glycerol, 0.5 mM dithiothreitol (DTT)), and were lysed using two passes in a microfluidizer at 10,000 PSI. Cell lysates were cleared by spinning at 16,000 RPM for 45 minutes in an Avanti JA-20 rotor. Cleared lysates were then run over a HisTrap HP column on an AKTA FPLC, washed with lysis buffer, and eluted with a gradient to 200 mM imidazole. RsbU was run on a Superdex200 16/600 column equilibrated with lysis buffer on an AKTA FPLC. Fractions were pooled and the 6-His tags were cleaved with 3C protease in dialysis to lysis buffer overnight at 4°C. Cleaved tags and 3C protease were subtracted by passing over a column containing equilibrated Ni-NTA resin. 2 mM EDTA was added to cleaved protein prior to gel filtration run. RsbU was then further purified on a Superdex200 16/600 column equilibrated with 20 mM K•HEPES pH 7.5, 100 mM NaCl, 2 mM DTT on an AKTA FPLC. Fractions were pooled, concentrated to 200 μM, and flash-frozen and stored at -80°C.

RsbT/U and RsbT/RsbU^{Q94L} co-expression

Cell pellets were resuspended in lysis buffer with 1 mM PMSF (50 mM K•HEPES pH 8.0, 200 mM NaCl, 20 mM imidazole, 10% glycerol, 0.5 mM DTT), and were lysed using two passes in a microfluidizer at 10,000 PSI. Cell lysates were cleared by spinning at 16,000 RPM for 45 minutes in an Avanti JA-20 rotor. Cleared lysates were then run over a HisTrap HP column on an AKTA FPLC, washed with lysis buffer, and eluted with a gradient to 200 mM imidazole. 2 mM EDTA was added to protein prior to gel filtration run. RsbT/RsbU was then further purified on a Superdex200 16/600 column equilibrated with 20 mM K•HEPES pH 8.0, 100 mM NaCl, 2 mM DTT on an AKTA FPLC. Fractions were pooled, concentrated to 200 μM, and flash-frozen and stored at -80°C.

RsbT

Cells were resuspended in lysis buffer with 1 mM PMSF (50 mM K•HEPES pH 8.0, 100 mM NaCl, 20 mM imidazole, 10% glycerol, 2 mM $MgCl_2$, 0.1 mM ATP, 0.5 mM DTT), and were lysed using two passes in a microfluidizer at 10,000 PSI. Cell lysates were cleared by spinning at 16,000 RPM for 45 minutes in an Avanti JA-20 rotor. Cleared lysates were then run over 2 mL/L of cells of Ni-NTA resin slurry equilibrated with lysis buffer. The resin was then washed with 10 CV of lysis buffer. Ni-NTA resin was resuspended with 10 mL of lysis buffer with 400 mM imidazole, and was incubated for 10 minutes. RsbT was eluted off column, elution was tracked by Bradford Reagent. Additional elution buffer was added until all protein was eluted off column. The 6-His tags were cleaved with 3C protease in dialysis to lysis buffer overnight at 4°C. Cleaved tags and 3C protease were subtracted by passing over a column containing equilibrated Ni-NTA resin. Protein was concentrated to approximately 50 uM, was flash-frozen and stored at -80°C.

RsbV

RsbV was expressed in *E. coli* BL21 (DE3) cells grown at 37°C to an OD_{600} of 0.4 and induced at 37°C for 3-4 hours with 1mM IPTG. Cells were harvested and resuspended in lysis buffer with 1 mM PMSF (50 mM K•HEPES pH 8.0, 200 mM NaCl, 20 mM imidazole, 10% glycerol, 0.5 mM DTT), and were lysed using two passes on a microfluidizer at 10,000 PSI. Cell lysates were cleared by spinning at 16,000 RPM for 45 minutes in an Avanti JA-20 rotor. Cleared lysates were then run over a HisTrap HP column on an AKTA FPLC, washed with lysis buffer, and eluted with a gradient to 200 mM imidazole. 2 mM EDTA was added to protein prior to gel filtration run. The 6-His tags were cleaved with 3C protease in dialysis to lysis buffer overnight at 4°C. Cleaved tags and 3C protease were subtracted by passing over a column containing equilibrated Ni-NTA resin. Cleaved protein was then further purified on a Superdex75 16/60 equilibrated in 20 mM K•HEPES pH 7.5, 150 mM NaCl, 10 % glycerol, 2 mM DTT. Fractions were pooled, concentrated to approximately 100 µM, and flash-frozen and stored at -80°C.

RsbW

Cell pellets were resuspended in lysis buffer with 1 mM PMSF (20 mM K•HEPES pH 7.5, 200 mM NaCl, 20 mM imidazole, 10 mM $MgCl_2$, 10 % glycerol, and 0.5 mM DTT), and were lysed using two passes on a microfluidizer at 10,000 PSI. Cell lysates were cleared by spinning at 16,000 RPM for 45 minutes in an Avanti JA-20 rotor. Cleared lysates were then run over a HisTrap HP column on an AKTA FPLC, washed with lysis buffer, and eluted with a gradient to 200 mM imidazole. The 6H tag was left uncleaved to aid removal after phosphorylation reactions. RsbW was then further purified on a Superdex75 16/60 equilibrated in 50 mM K•HEPES pH 7.5, 150 mM NaCl, 10% glycerol, and 2 mM DTT. Fractions were pooled, concentrated to approximately 100 µM, and flash-frozen and stored at -80°C.

RsbV-P

RsbVW coexpression plasmid was expressed in *E. coli* BL21 (DE3) cells grown at 37°C to an OD_{600} of 0.4 and induced at 37°C for 3-4 hours with 1mM IPTG. Cells were harvested and resuspended in lysis buffer with 1 mM PMSF (50 mM K•HEPES pH 7.5, 50 mM KCl, 20 mM imidazole, 0.5 mM DTT), and were lysed using two passes on a microfluidizer at 10,000 PSI. Cell lysates were cleared by spinning at 16,000 RPM for 45 minutes in an Avanti JA-20 rotor. Cleared lysates were then run over a HisTrap HP column on an AKTA FPLC, washed with lysis buffer, and eluted with a gradient to 200 mM imidazole. The 6-His tags were cleaved with 3C protease in dialysis to lysis buffer overnight at 4°C. Cleaved tags and 3C protease were subtracted by passing over a column containing equilibrated Ni-NTA resin. RsbVW was run on a Superdex75 16/60 column equilibrated with lysis buffer on an AKTA FPLC. Fractions of RsbVW coelution were pooled and RsbV was phosphorylated in dialysis at room temperature in lysis buffer with 5 mM ATP and 10 mM $MgCl_2$.

RsbV-P Fractions were pooled, concentrated to 200 µM, and flash-frozen and stored at -80°C. Dialyzed RsbVW were then concentrated and run on Superdex75 16/60 column equilibrated with 20 mM K•HEPES pH 7.5, 150 mM NaCl, 10% glycerol, 2 mM DTT. RsbV-P Fractions were pooled, concentrated to 200 µM, and flash-frozen and stored at -80°C.

SEC-MALS-SAXS

Small Angle X-ray Scattering (SAXS) was performed at BioCAT (beamline 18ID at the Advanced Photon Source, Chicago) with in-line size exclusion chromatography (SEC) to separate sample from aggregates and other contaminants and ensure optimal sample quality. In-line multiangle light scattering (MALS), dynamic light scattering (DLS) and differential refractive index (dRI) measurements were recorded for additional biophysical characterization (SEC-MALS-SAXS). The samples were loaded on a Superdex 200 10/300 Increase GL Column (Cytiva) run by a 1260 Infinity II HPLC (Agilent Technologies) at 0.6 ml/min. The flow passed in order through an Agilent UV detector, a MALS detector and a DLS detector (DAWN Helios II, Wyatt Technologies), and an RI detector (Optilab T-rEX, Wyatt) before the SAXS flow cell. The flow cell consists of a 1.0 mm ID quartz capillary with ~20 µm walls. A coflowing buffer sheath is used to separate sample from the capillary walls, helping prevent radiation damage (Kirby et al. 2016). Scattering intensity was recorded using a Pilatus3 X 1M (Dectris) detector that was placed 3.682 m from the sample giving us access to a q-range of 0.0027 $Å^{-1}$ to 0.33 $Å^{-1}$. 0.5s exposures were acquired every 1 s during elution and data was reduced using BioXTAS RAW 2.1.4 (Hopkins et al. 2017) (Hopkins 2024). Buffer blanks were created by averaging regions flanking the elution peak and subtracted from all measured profiles. Because of the heterogeneity in the samples, evolving factor analysis (EFA) was used to deconvolve the scattering profiles of the overlapping components (Meisburger et al. 2016). These scattering profiles were used for subsequent analysis in RAW. The quality of the deconvolution was assessed based on the mean weighted χ^2 for each deconvoluted component and the χ^2 of the combined fit to each frame of the dataset (**Figure 4 – Figure Supplement 2B-E**, **Figure 4 – Figure Supplement 4B-E**). RAW was used to run GNOM from the ATSAS package (version 3.2.1) (Svergun 1992; Manalastas-Cantos et al. 2021). Description of each SAXS sample and results of the analysis are presented in Table 1 (Trewhella et al. 2017).The composition of each scattering component was determined based on the SAXS derived molecular weights, the MALS profile, and gels from the purification of the protein or protein complex (**Figure 4 – Figure Supplement 1**; Table 1). Molecular weights and hydrodynamic radii were calculated from the MALS and DLS data respectively using the ASTRA 7 software (Wyatt). All samples were run in 20 mM HEPES pH 7.5, 100 mM NaCl, 5 mM DTT. Wild-type RsbU was run at a concentration of 3.5 mg/mL, RsbT/$RsbU^{Q94L}$ was run at a concentration of 2.5 mg/mL, $RsbU^{Q94L}$ was run at a concentration of 3.5 mg/mL, RsbT/RsbU was run at a concentration of 2.5 mg/mL. FoXS was used to calculated predicted scattering profiles from the model, and was compared to the experimental scattering profiles (Schneidman-Duhovny et al. 2016; Schneidman-Duhovny et al. 2013). Output parameters calculated using FoXS are provided in Table 1. MultiFoXS was used to generate a flexible structure ensemble with multicomponent fits and was compared to the experimental scattering profiles (Schneidman-Duhovny et al. 2016). MultiFoXS input and output parameters are provided in Table 1.

Fluorescence anisotropy

We site-specifically labeled RsbT with tetramethylrhodamine 5-maleimide (TMR) dye at its unique cysteine (position 6). We added increasing concentrations of RsbU and $RsbU^{Q94L}$ to 200nM $RsbT^{TMR}$ and measured the change in anisotropy (**Figure 2A**). All measurements were done at 25°C in 50 mM K•HEPES pH 7.5, 100 mM NaCl, and 10% glycerol. All measurements of spectra were conducted with a slit width of 7 nm, and anisotropy measurements were conducted with a slit width of 7 nm. The excitation wavelength was 551 nm and the emission wavelength was 577 nm. Anisotropy measurements were taken 30 seconds apart for 6 measurements, and then were averaged and plot against its corresponding concentration of RsbU. Anisotropy data was then fit to a quadratic binding curve using KaleidaGraph, reported errors are the error of the fit.

Phosphatase assays

Phosphatase assays were performed with RsbV-P that was labeled with ^{32}P by incubating RsbV (40 μM), 6His-RsbW (45 μM), and 100 μCi of γ-^{32}P ATP overnight at room temperature in 50 mM K•HEPES pH 7.5, 50 mM KCl, 10 mM $MgCl_2$, and 2 mM DTT. Unincorporated nucleotide was removed by buffer exchange using a Zeba spin column equilibrated in 50 mM K•HEPES pH 8.0, 100 mM NaCl. 6H-RsbW was then removed by Ni-NTA resin equilibrated in 50 mM K•HEPES pH 8.0, 100 mM NaCl, 20 mM imidazole. The flow-through fraction from the Ni-NTA resin containing RsbV-^{32}P was then exchanged into 50 mM K•HEPES pH 8.0, 100 mM NaCl buffer using 3 subsequent Zeba spin columns to remove all unincorporated nucleotide and free phosphate. Labeled RsbV-^{32}P was aliquoted and frozen at -80°C for future use.

All phosphatase assays were performed at room temperature in 50 mM K•HEPES pH 7.5, 100 mM NaCl. The concentrations of enzyme, substrate, $MnCl_2$, and $MgCl_2$ were varied as indicated. 10 μM RsbT was additionally added to reactions as indicated. Reactions were stopped with 0.5 M EDTA, pH 8.0 and run on PEI-Cellulose TLC plates developed in 1 M $LiCl_2$ and 0.8 M acetic acid and imaged on a Typhoon scanner. Phosphatase assays were performed more than three independent times as separate experiments. Data shown in figures is from a single representative experiment, and reported errors are the error from the fit.

B. subtilis strain construction

B. subtilis cells were grown in Lennox lysogeny broth (LB, Sigma Aldrich) as liquid medium or as plates supplemented with 15% Bacto Agar (Difco). Antibiotics were used as appropriate for maintenance of plasmids or for selection of transformants: MLS (50 μg/ml erythromycin, 250 μg/ml lincomycin), kanamycin (10 μg/ml). For plates used to visualize σ^B reporter activity, 80 μg/ml of 5-bromo-4-chloro-3-indolyl-β-D-galactopyranoside (X-gal) and 1 mM IPTG were added. All *B. subtilis* strains were derived from the PY79 strain background and are listed in the table of strains. Plasmids based on pHB201(Bron et al. 1998) were introduced to *B. subtilis* strains using natural competence(Harwood & Cutting 1990).

Genetic screens

Genetic screens were performed as described previously (Ho & Bradshaw 2021). Plasmids containing *rsbU* or *rsbT/rsbU*^{Y28I} were subjected to PCR mutagenesis using GoTaq DNA polymerase mix (Promega) supplemented with 2mM additional $MgCl_2$. Pools of mutagenized inserts were assembled into digested plasmid using isothermal (Gibson) assembly and transformed into *E. coli* DH5α cells. Mutation rate of approximately one single-nucleotide polymorphism per kilobase of DNA was confirmed by sequencing individual clones. Plasmids were then introduced to *B. subtilis* using natural competence and cells were plated on selective medium containing IPTG and X-gal for two days at 37°C. Blue colonies were selected, restruck on plates with and without IPTG, and plasmids recovered from single colonies that retested as σ^B positive were sequenced using Sanger sequencing. For the RsbU^{Y28I} suppressor screen, two independent pools of PCR mutagenized plasmid were screened. In addition to the reported variants that were selected, we identified simple revertants that restored Y28 in both pools, and mutations in the promoter and RBS that we predict enhanced protein production. These variants were not studied further. Individual amino acid changing mutations were rebuilt in the parental plasmid using PCR (QuickChange) mutagenesis and the phenotypes were validated by replating on indicator plates. All strains shown in the figures are from these rebuilt plasmids.

AlphaFold2 structure predictions

AlphaFold2 predictions were performed using ColabFold (Mirdita et al. 2022). Alphafold2_multimer_v2 was used in unpaired_paired mode with no templates with 3 recycles, 200 iterations, and greedy pairing strategy. The predicted aligned error plots for all AlphaFold2

structures are shown in **Figure 1 – Figure Supplement 1**. The predicted local distance difference test scores (pLDDT) mapped onto the structures are shown in **Figure 1 – Figure Supplement 2**.

Socket2 analysis of AlphaFold2 structure predictions

Socket2 coiled-coil predictions were performed using Socket2 Colab (Kumar & Woolfson 2021). Socket2 was used with a packing cutoff of 7.0Å. Analysis done using Socket2 is shown in **Figure 5 – Figure Supplement 2**.

Acknowledgements

The authors thank Richard Losick, Dorothee Kern, Chris Miller, Julia Kardon, Matthew Cabeen, Liz Hedstrom, Susan Lovett, Emily Stadnicki, and Maria-Eirini Pandelia for input at various stages of this project. Justin Curran, LuYing Pan, Spencer Clark, Alexis Ryan, and Wendy Yang additionally contributed to the research. This research was supported by startup funds to NB from Brandeis University. RB was supported by T32 GM135126 and SP was supported by T32 GM007122. This research used resources of the Advanced Photon Source, a U.S. Department of Energy (DOE) Office of Science User Facility operated for the DOE Office of Science by Argonne National Laboratory under Contract No. DE-AC02-06CH11357. BioCAT was supported by grant P30 GM138395 from the National Institute of General Medical Sciences of the National Institutes of Health. Use of the Pilatus 3 1M detector was provided by grant 1S10OD018090 from NIGMS. The content is solely the responsibility of the authors and does not necessarily reflect the official views of the National Institute of General Medical Sciences or the National Institutes of Health.

Additional information

Author contributions

RB, conceptualization, investigation, data analysis, visualization, writing-original draft, writing-review and editing. KH, PR, conceptualization, data analysis, investigation. JH, investigation, data analysis, writing-review and editing. MW, SLR, SCP, LC, investigation. NB, conceptualization, visualization, writing-original draft, writing-review editing, and supervision.

References

Bartolini M., et al. 2019) **Regulation of Biofilm Aging and Dispersal in Bacillus subtilis by the Alternative Sigma Factor SigB** *Journal of Bacteriology* **201**

Battesti A., et al. 2013) **Anti-adaptors provide multiple modes for regulation of the RssB adaptor protein** *Genes & development* **27**:2722–2735

Battesti A., Majdalani N., Gottesman S. 2015) **Stress sigma factor RpoS degradation and translation are sensitive to the state of central metabolism** *Proceedings of the National Academy of Sciences of the United States of America*

Battesti A., Majdalani N., Gottesman S. 2011) **The RpoS-mediated general stress response in Escherichia coli** *Annual review of microbiology* **65**:189–213

Bergkessel M., Basta D.W., Newman D.K. 2016) **The physiology of growth arrest: uniting molecular and environmental microbiology** *Nature Reviews Microbiology* **14**:549–562

Bilwes A.M., et al. 1999) **Structure of CheA, a signal-transducing histidine kinase** *Cell* **96**:131–141

Boekhoud I.M., et al. 2020) **Redefining the Clostridioides difficile σB Regulon: σB Activates Genes Involved in Detoxifying Radicals That Can Result from the Exposure to Antimicrobials and Hydrogen Peroxide** *mSphere* **5**

Boylan S.A., Redfield A.R., Price C.W. 1993) **Transcription factor sigma B of Bacillus subtilis controls a large stationary-phase regulon** *Journal of Bacteriology* **175**:3957–3963

Bradshaw N., et al. 2017) **A widespread family of serine/threonine protein phosphatases shares a common regulatory switch with proteasomal proteases** *eLife* **6**

Brody M.S., Stewart V., Price C.W. 2009) **Bypass suppression analysis maps the signalling pathway within a multidomain protein: the RsbP energy stress phosphatase 2C from Bacillus subtilis** *Molecular microbiology* **72**:1221–1234

Bron S., et al. 1998) **Protein secretion and possible roles for multiple signal peptidases for precursor processing in bacilli** *Journal of biotechnology* **64**:3–13

Brugger C., Schwartz J., et al. 2023) **Structure of phosphorylated-like RssB, the adaptor delivering σs to the ClpXP proteolytic machinery, reveals an interface switch for activation** *The Journal of biological chemistry* **299**:105440

Brugger C., Srirangam S., Deaconescu A.M. 2023) **IraM Remodels the RssB Segmented Helical Linker to Stabilize σs Against Degradation by ClpXP** *The Journal of biological chemistry* :105568

Chakravarty D., Porter L.L. 2022) **AlphaFold2 fails to predict protein fold switching** *Protein Science* **31**:e4353

Cordeiro T.N., et al. 2017) **Structural Characterization of Highly Flexible Proteins by Small-Angle Scattering** *Advances in experimental medicine and biology* **1009**:107–129

de Been M., et al. 2010) **A novel hybrid kinase is essential for regulating the sigma(B)-mediated stress response of Bacillus cereus** *Environmental microbiology* **12**:730–745

Delumeau O., et al. 2004) **Functional and structural characterization of RsbU, a stress signaling protein phosphatase 2C** *J Biol Chem.* **279**:40927–40937

Dorich V., et al. 2019) **Structural basis for inhibition of a response regulator of σS stability by a ClpXP antiadaptor** *Genes & development* **33**:718–732

Fernández Martínez L., et al. 2009) **Osmoregulation in Streptomyces coelicolor: modulation of SigB activity by OsaC** *Molecular microbiology* **71**:1250–1262

Galperin M.Y 2006) **Structural classification of bacterial response regulators: diversity of output domains and domain combinations** *J Bacteriol.* **188**:4169–4182

Gottesman S 2019) **Trouble is coming: Signaling pathways that regulate general stress responses in bacteria** *J Biol Chem.* **294**:11685–11700

Gourinchas G., et al. 2017) **Long-range allosteric signaling in red light-regulated diguanylyl cyclases** *Science advances* **3**:e1602498

Greenstein A.E., et al. 2009) **Interdomain communication in the Mycobacterium tuberculosis environmental phosphatase Rv1364c** *J Biol Chem.* **284**:29828–29835

Grigoryan G., DeGrado W.F. 2011) **Probing designability via a generalized model of helical bundle geometry** *J Mol Biol.* **405**:1079–1100

Guerreiro D.N., Arcari T., O'Byrne C.P. 2020) **The σB-Mediated General Stress Response of Listeria monocytogenes: Life and Death Decision Making in a Pathogen** *Frontiers in microbiology* **11**:1505

Guldimann C., et al. 2016) **Resilience in the face of uncertainty: sigma B fine-tunes gene expression to support homeostasis in Gram-positive bacteria** *Applied and Environmental Microbiology* **82**:4456–4469

Haldenwang W.G., Losick R. 1979) **A modified RNA polymerase transcribes a cloned gene under sporulation control in Bacillus subtilis** *Nature* **282**:256–260

Hardwick S.W., et al. 2007) **Structural and functional characterization of partner switching regulating the environmental stress response in Bacillus subtilis** *J Biol Chem.* **282**:11562–11572

Harms A., Maisonneuve E., Gerdes K. 2016) **Mechanisms of bacterial persistence during stress and antibiotic exposure** *Science* **354**:aaf4268–aaf4268

Harwood C.R., Cutting S.M. 1990) **Molecular Biological Methods for Bacillus** John Wiley & Sons Ltd pp. 1–308

Hecker M., Pané-Farré J., Völker U. 2007) **SigB-dependent general stress response in Bacillus subtilis and related gram-positive bacteria** *Annual review of microbiology* **61**:215–236

Heinz V., et al. 2022) **The Vibrio vulnificus stressosome is an oxygen-sensor involved in regulating iron metabolism** *Communications biology* **5**:622

Herbert S., et al. 2010) **Repair of global regulators in Staphylococcus aureus 8325 and comparative analysis with other clinical isolates** *Infection and immunity* **78**:2877–2889

Ho K., Bradshaw N. 2021) **A conserved allosteric element controls specificity and activity of functionally divergent PP2C phosphatases from B. subtilis** *The Journal of biological chemistry* :100518

Hopkins J.B., Gillilan R.E., Skou S. 2017) **BioXTAS RAW: improvements to a free open-source program for small-angle X-ray scattering data reduction and analysis** *Journal of applied crystallography* **50**:1545–1553

Jumper J., et al. 2021) **Highly accurate protein structure prediction with AlphaFold** *Nature* **596**:583–589

Kikhney A.G., Svergun D.I. 2015) **A practical guide to small angle X-ray scattering (SAXS) of flexible and intrinsically disordered proteins** *FEBS letters* **589**:2570–2577

Kint N., et al. 2017) **The alternative sigma factor σ(B) plays a crucial role in adaptive strategies of Clostridium difficile during gut infection** *Environmental microbiology*

Kint N., et al. 2019) **The σB signalling activation pathway in the enteropathogen Clostridioides difficile** *Environmental microbiology* **21**:2852–2870

Kirby N., et al. 2016) **Improved radiation dose efficiency in solution SAXS using a sheath flow sample environment. Acta crystallographica. Section D** *Structural biology* **72**:1254–1266

Kumar P., Woolfson D.N. 2021) **Socket2: a program for locating, visualizing and analyzing coiled-coil interfaces in protein structures** *Bioinformatics (Oxford, England)* **37**:4575–4577

Manalastas-Cantos K., et al. 2021) **ATSAS 3.0: expanded functionality and new tools for small-angle scattering data analysis** *Journal of applied crystallography* **54**:343–355

Marles-Wright J., et al. 2008) **Molecular architecture of the "stressosome," a signal integration and transduction hub** *Science* **322**:92–96

Meisburger S.P., et al. 2016) **Domain Movements upon Activation of Phenylalanine Hydroxylase Characterized by Crystallography and Chromatography-Coupled Small-Angle X-ray Scattering** *Journal of the American Chemical Society* **138**:6506–6516

Mirdita M., et al. 2022) **ColabFold: making protein folding accessible to all** *Nature methods* **19**:679–682

Mittenhuber G. 2002) **A phylogenomic study of the general stress response sigma factor sigmaB of Bacillus subtilis and its regulatory proteins** *Journal of Molecular Microbiology and Biotechnology* **4**:427–452

Möglich A., Ayers R.A., Moffat K. 2009) **Structure and signaling mechanism of Per-ARNT-Sim domains** *Structure (London, England : 1993)* **17**:1282–1294

Nadezhdin E.V., Brody M.S., Price C.W. 2011) **An α/β Hydrolase and Associated Per-ARNT-Sim Domain Comprise a Bipartite Sensing Module Coupled with Diverse Output Domains** *PLoS*

ONE **6**:e25418

Quin M.B, et al. 2012) **The bacterial stressosome: a modular system that has been adapted to control secondary messenger signaling** *Structure (London, England : 1993)* **20**:350–363

Rambo R.P., Tainer J.A. 2011) **Characterizing flexible and intrinsically unstructured biological macromolecules by SAS using the Porod-Debye law** *Biopolymers* **95**:559–571

Randall T.E., et al. 2022) **Sensory Perception in Bacterial Cyclic Diguanylate Signal Transduction** *Journal of Bacteriology* **204**:e0043321

Receveur-Bréchot V., Durand D. 2012) **How random are intrinsically disordered proteins? A small angle scattering perspective** *Current protein & peptide science* **13**:55–75

Rodríguez-Martínez K., et al. 2023) **Defining the regulatory mechanisms of sigma factor RpoS degradation in Azotobacter vinelandii and Pseudomonas aeruginosa** *Molecular microbiology* **120**:91–102

Schneidman-Duhovny D., et al. 2013) **Accurate SAXS profile computation and its assessment by contrast variation experiments** *Biophysical journal* **105**:962–974

Schneidman-Duhovny D., et al. 2016) **FoXS, FoXSDock and MultiFoXS: Single-state and multi-state structural modeling of proteins and their complexes based on SAXS profiles** *Nucleic Acids Research* **44**:W424–9

Svergun D.I. 1992) **Determination of the regularization parameter in indirect-transform methods using perceptual criteria** *Journal of applied crystallography* **25**:495–503

Trewhella J., et al. 2017) **2017 publication guidelines for structural modelling of small-angle scattering data from biomolecules in solution: an update** *Acta crystallographica. Section D, Structural biology* **73**:710–728

Tuchscherr L., Löffler B. 2016) **Staphylococcus aureus dynamically adapts global regulators and virulence factor expression in the course from acute to chronic infection** *Current genetics* **62**:15–17

Vijay K., et al. 2000) **A PP2C phosphatase containing a PAS domain is required to convey signals of energy stress to the sigmaB transcription factor of Bacillus subtilis** *Molecular microbiology* **35**:180–188

Yang X., et al. 1996) **Opposing pairs of serine protein kinases and phosphatases transmit signals of environmental stress to activate a bacterial transcription factor** *Genes & development* **10**:2265–2275

Zschiedrich C.P., Keidel V., Szurmant H. 2016) **Molecular Mechanisms of Two-Component Signal Transduction** *J Mol Biol.* **428**:3752–3775

Author information

Rishika Baral
Department of Biochemistry, Brandeis University, Waltham, United States, Graduate program in Biochemistry and Biophysics, Brandeis University, Waltham, United States
ORCID iD: 0000-0002-9365-8877

Kristin Ho
Department of Biochemistry, Brandeis University, Waltham, United States
ORCID iD: 0000-0002-2063-7127

Ramasamy P Kumar
Department of Biochemistry, Brandeis University, Waltham, United States
ORCID iD: 0000-0002-6555-8289

Jesse B Hopkins
Biophysics Collaborative Access Team (BioCAT), Department of Physics, Illinois Institute of Technology, Chicago, United States
ORCID iD: 0000-0001-8554-8072

Maxwell B Watkins
Biophysics Collaborative Access Team (BioCAT), Department of Biology, Illinois Institute of Technology, Chicago, United States
ORCID iD: 0000-0003-4559-2049

Salvatore LaRussa
Department of Biochemistry, Brandeis University, Waltham, United States, Graduate program in Biochemistry and Biophysics, Brandeis University, Waltham, United States
ORCID iD: 0000-0003-4749-1356

Suhaily Caban-Penix
Department of Biochemistry, Brandeis University, Waltham, United States, Graduate program in Molecular and Cell Biology, Brandeis University, Waltham, United States

Logan A Calderone
Department of Biochemistry, Brandeis University, Waltham, United States, Graduate program in Biochemistry and Biophysics, Brandeis University, Waltham, United States
ORCID iD: 0000-0002-0960-3831

Niels Bradshaw
Department of Biochemistry, Brandeis University, Waltham, United States
ORCID iD: 0000-0002-6845-4717

For correspondence: niels@brandeis.edu

Editors

Reviewing Editor
Karine Gibbs
University of California, Berkeley, Berkeley, United States of America

Senior Editor
Dominique Soldati-Favre
University of Geneva, Geneva, Switzerland

Reviewer #1 (Public review):

Summary:

This very interesting manuscript proposes a general mechanism for how activating signaling proteins respond to species specific signals arising from a variety of stresses. In brief, the authors propose that the activating signal alters the structure by a universal allosteric mechanism.

Strengths:

The unitary mechanism proposed is appealing and testable. The propose that the allosteric module consists of crossed alpha-helical linkers with similar architecture and that their attached regulatory domains connect to phosphatases or other molecules through coiled-coli domains, such that the signal is transduced via rigidifying the alpha helices, permitting downstream enzymatic activity. The authors present genetic and structural prediction data in favor of the model for the system they are studying, and stronger structural data in other systems.

Weaknesses:

I thank the authors for making significant revisions that addressed almost all of my concerns. I hope that the authors will consider addressing my last concern, which is that the title is inappropriate. However, I do not believe that this should hold up the publication of the ms.

"A General Mechanism for Initiating the General Stress Response in Bacteria" is misleading because it suggests a broadly applicable, universal mechanism across all bacterial species, whereas the study primarily focuses on Bacillus subtilis and its RsbU phosphatase activation. While the authors propose that the mechanism may extend to other bacteria, the evidence is largely based on structural modeling rather than direct experimental validation across multiple phyla. Additionally, the phrase "General Stress Response" might imply that the paper broadly explains stress response regulation, but it specifically examines the activation of RsbU by RsbT, which is just one really small part of the broader GSR network. The redundancy in "A General Mechanism for the General Stress Response" could also create an impression of an oversimplified, universal model when stress responses are often species- and context-specific. Furthermore, the study builds upon existing knowledge of partner-switching mechanisms rather than introducing an entirely new concept, making the claim of a general mechanism overstated and misleading for the field.

Title options could be "A Conserved Activation Mechanism for the General Stress Response Phosphatase in Bacteria", "Coiled-Coil Linker-Mediated Activation of a General Stress Response Phosphatase", all of which more accurately reflect the study's scope and findings.

https://doi.org/10.7554/eLife.100376.2.sa3

Reviewer #2 (Public review):

Summary:

While bacteria have the ability to induce genes in response to specific stresses, they also use the General Stress Response (GSR) to deal with growth conditions that presumably include a larger range of stresses (for instance, stationary phase growth). The activation of GSR-specific

sigma factors is frequently at the heart of the induction of a GSR. Given the range of stresses that can lead to GSR induction, the regulatory inputs are frequently complex. In B. subtilis, the stressosome, a multi-protein complex, contains a set of proteins that, upon appropriate stresses, initiate partner switching cascades that free the sigma B sigma factor from an anti-sigma. The focus here is on the mode of activation of RsbU, a serine/threonine phosphatase of the PPM family, leading to sigB activation. RbsT, a component of the degradosome interacts with RsbU upon stress, activating the phosphatase activity. Once active, RsbU dephosphorylates its target (RsbV, an anti-antisigma), which in turn binds the anti-sigma. The conclusion is that flexible linker domains upstream of the phosphatase domain are the target for activation, resulting in a crossed-linker dimeric structure. The authors then use the information on RsbU to suggest that parallel approaches may be used to activate PPM phosphatases for the GSR response in other bacteria.

Strengths and Weaknesses:

(1) A strength of the work is the combination of modeling, genetics and biochemical approaches to support the idea that the flexibility of the linker of the RsbU phosphatase is critical to signalling and that this changes as a result of interactions of the signaling protein RsbT.

(2) The impact of the work, beyond better understanding of this particular signalling system, lies in the suggested parallels with other GSR system regulators in a range of bacteria. The work here provides fairly clear indications of what mutational changes would be most likely to test the model.

(3) Assuming that these predictions are shown to be correct in future work, that will leave as an intriguing question why this particular geometry has been conserved in GSR - whether they emerge from a common ancestor (found where?) and/or there is some characteristic (flexibility of modulating the response?) that is particularly important for GSR signal input. Coupled with this will be further understanding of how the linker and/or interacting proteins change in different systems.

https://doi.org/10.7554/eLife.100376.2.sa2

Reviewer #3 (Public review):

Summary:

The authors present a study building on their previous work on activation of the general stress response phosphatase, RsbU, from Bacillus subtilis. Using computed structural models of the RsbU dimer the authors map previously identified activating mutations onto the structure and suggest further protein variants to test the role of the predicted linker helix and the interaction with RsbT on the activation of the phosphatase activity.

Using in vivo and in vitro activity assays, the authors demonstrate that linker variants can constitutively activate RsbU and increase the affinity of the protein for RsbT, thus showing a link between the structure of the linker region and RsbT binding.

Small angle X-ray scattering experiments on RsbU variants alone, and in complex with RsbT show structural changes consistent with a decreased flexibility of the RsbU protein, which are hypothesised to indicate an disorder-order transition in the linker when RsbT binds. This interpretation of the data is consistent with the biochemical data presented by the authors.

Further computed structure models are presented for other protein phosphates from different bacterial species and the authors propose a model for phosphatase activation by partner binding. They compare this to the activation mechanisms proposed for histidine

kinase two-component systems and GGDEF proteins and suggest the individual domains could be swapped to give a toolkit of modular parts for bacterial signalling.

Strengths:

The key mutagenesis data is presented with two lines of evidence to demonstrate RsbU activation - in vivo sigma-b activation assays utilising a beta-galactosidase reporter and in vitro activity assays against the RsbV protein, which is the downstream target of RsbU. These data support the hypothesis for RsbT binding to the RsbU linker region as well as the dimerisation domain to activate the RsbU activity.

Weaknesses:

Small angle scattering curves are difficult to unambiguously interpret, but the authors present good interpretations that fit with the biochemical data presented. These interpretations should be considered as models for future testing with other methods - hydrogen/deuterium exchange mass spectrometry, would be a good additional method to use, as exchange rates in the linker region would be affected significantly by the disorder/order transition on RsbT binding.

The interpretation of the computed structure models is provided with a few caveats related to the bias in the models returned by AlphaFold2. For the full-length models of RsbU and other phosphatase proteins, the relationship of the domains to each other is likely to be the least reliable part of the models - this is apparent from the PAE plots shown in supplementary figure 8.

Comments on revisions:

The authors have addressed the review comments satisfactorily for this manuscript to stand as a version of record.

https://doi.org/10.7554/eLife.100376.2.sa1

Author response:

The following is the authors' response to the original reviews

> ***Public reviews:***
>
> ***Reviewer #1 (Public review):***
>
> *Summary:*
>
> *This very interesting manuscript proposes a general mechanism for how activating signaling proteins respond to species-specific signals arising from a variety of stresses. In brief, the authors propose that the activating signal alters the structure by a universal allosteric mechanism.*
>
> *Strengths:*
>
> *The unitary mechanism proposed is appealing and testable. They propose that the allosteric module consists of crossed alpha-helical linkers with similar architecture and that their attached regulatory domains connect to phosphatases or other molecules through coiled-coli domains, such that the signal is transduced via rigidifying the alpha helices, permitting downstream enzymatic activity. The authors present genetic and structural prediction data in favor of the model for the system they are studying, and stronger structural data in other systems.*

> *Weaknesses:*
>
> *The evidence is indirect - targeted mutations, structural predictions, and biochemical data. Therefore, these important generalizable conclusions are not buttressed by impeccable data, which would require doing actual structures in B. subtilis, confirming experiments in other organisms, and possibly co-evolutionary coupling. In the absence of such data, it is not possible to rule out variant models.*

We thank the reviewer for their feedback. A challenge of studying flexible proteins is that it is often not possible to directly obtain high resolution structural data. For the case of *B. subtilis* RsbU, the independent experimental approaches we applied (including two unbiased genetic screens, targeted mutagenesis, SAXS, enzymology, and structure prediction, which includes evolutionary coupling) converged upon a model for activation, which we feel is well supported. Frustratingly, our attempts at determining high resolution experimental structures have been unsuccessful, which we think is due to the flexibility of the proteins revealed by our SAXS experiments. For example, we collected X-ray diffraction data from crystals of a fragment of *B. subtilis* RsbU containing the N-terminal domain and linker in which the linker was almost entirely disordered in the maps. We agree that doing experiments in other organisms would be valuable next steps to test the hypothesis that this coiled-coil based transduction mechanism is conserved across species, and will modify the text to differentiate this more speculative section of the manuscript.

We have modified the abstract to read:

“This coiled-coil linker transduction mechanism additionally suggests a resolution to the mystery of how shared sensory domains control serine/threonine phosphatases, diguanylate cyclases and histidine kinases.”

We have modified the results to read:

"These predictions suggest a testable hypothesis that RsbP is controlled through an activation mechanism similar to that of RsbU (Fig. 5A)”

“From this analysis, we speculate that linker-mediated phosphatase domain dimerization is an evolutionarily conserved, adaptable mechanism to control PPM phosphatase activity.”

Based on this critique (and the critiques of the other reviewers), we plan to do energetic analysis of the predicted coiled coils from the enzymes we analyzed from other species and to incorporate this into the manuscript.

We have modified the results to read:

Consistent with a model in which the stability of the linker plays a conserved regulatory role, the AlphaFold2 models for many of the predicted structures have unfavorable polar residues buried in the coiled-coil interface (positions a and d, for which non-polar residues are most favorable) (Figure 5 – figure supplement 2).”

Finally, in the manuscript, we have highlighted that this mechanism is not the only mechanism for activation of other proteins with effector domains connected to linkers, but rather one of many mechanisms (Fig 5G). The reviewer additionally made helpful suggestions about the text in detailed comments that we will incorporate as appropriate.

> ***Reviewer #2 (Public review):***
>
> *Summary:*

> *While bacteria have the ability to induce genes in response to specific stresses, they also use the General Stress Response (GSR) to deal with growth conditions that presumably include a larger range of stresses (for instance, stationary phase growth). The activation of GSR-specific sigma factors is frequently at the heart of the induction of a GSR. Given the range of stresses that can lead to GSR induction, the regulatory inputs are frequently complex. In B. subtilis, the stressosome, a multi-protein complex, contains a set of proteins that, upon appropriate stresses, initiate partner switching cascades that free the sigma B sigma factor from an anti-sigma. The focus here is on the mode of activation of RsbU, a serine/threonine phosphatase of the PPM family, leading to sigB activation. RbsT, a component of the degradosome interacts with RsbU upon stress, activating the phosphatase activity. Once active, RsbU dephosphorylates its target (RsbV, an anti-antisigma), which in turn binds the anti-sigma. The conclusion is that flexible linker domains upstream of the phosphatase domain are the target for activation, via binding of proteins to the N-terminal domain, resulting in a crossed-linker dimeric structure. The authors then use the information on RsbU to suggest that parallel approaches are used to activate PPM phosphatases for the GSR response in other bacteria. (Biology vs. Mechanism, evolution?)*
>
> *Strengths and Weaknesses:*
>
> *Many of these have to do with clarifying what was done and why. This includes the presentation and content of the figures.*
>
> *One issue relates to the background and context. A bit more information on the stresses that release RsbT would be useful here. The authors might also consider a figure showing the major conclusions and parallels for SpoIIE activation and possibly other partner switches that are discussed, introducing the switch change more clearly to set the stage for the work here (and the generalization). There are a lot of players to keep track of.*

We plan to carefully review the manuscript to improve the clarity of presentation and background. In particular, we thank the reviewer for pointing out the missing information about the release of RsbT from the stressosome. We will incorporate this information into the introduction and provide an additional figure.

We have added the following text to the introduction:

“RsbT is sequestered in a megadalton stress sensing complex called the stressosome, and is released to bind RsbU in response to specific stress signals including ethanol, heat, acid, salt, and blue light”

We have added a new figure panel (2C) that shows the model for how Q94L, M166V, and RsbT binding induce conformational change of the PPM domain to recruit metal cofactor and activate RsbU (analogous, but slightly different from the mechanism for SpoIIE).

The reviewer additionally provided detailed helpful comments that we will incorporate in the text and figures.

> ***Reviewer #3 (Public review):***
>
> *Summary:*
>
> *The authors present a study building on their previous work on activation of the general stress response phosphatase, RsbU, from Bacillus subtilis. Using computed structural models of the RsbU dimer the authors map previously identified activating mutations onto the structure and suggest further protein variants to test the role of the predicted linker helix and the interaction with RsbT on the activation of the phosphatase activity.*

> *Using in vivo and in vitro activity assays, the authors demonstrate that linker variants can constitutively activate RsbU and increase the affinity of the protein for RsbT, thus showing a link between the structure of the linker region and RsbT binding.*
>
> *Small angle X-ray scattering experiments on RsbU variants alone, and in complex with RsbT show structural changes consistent with a decreased flexibility of the RsbU protein, which is hypothesised to indicate a disorder-order transition in the linker when RsbT binds. This interpretation of the data is consistent with the biochemical data presented by the authors.*
>
> *Further computed structure models are presented for other protein phosphates from different bacterial species and the authors propose a model for phosphatase activation by partner binding. They compare this to the activation mechanisms proposed for histidine kinase two-component systems and GGDEF proteins and suggest the individual domains could be swapped to give a toolkit of modular parts for bacterial signalling.*
>
> *Strengths:*
>
> *The key mutagenesis data is presented with two lines of evidence to demonstrate RsbU activation - in vivo sigma-b activation assays utilising a beta-galactosidase reporter and in vitro activity assays against the RsbV protein, which is the downstream target of RsbU. These data support the hypothesis for RsbT binding to the RsbU linker region as well as the dimerisation domain to activate the RsbU activity.*
>
> *Weaknesses:*
>
> *Small angle scattering curves are difficult to unambiguously interpret, but the authors present reasonable interpretations that fit with the biochemical data presented. These interpretations should be considered as good models for future testing with other methods - hydrogen/deuterium exchange mass spectrometry, would be a good additional method to use, as exchange rates in the linker region would be affected significantly by the disorder/order transition on RsbT binding.*

We agree with the reviewer that the SAXS data has inherent ambiguity due to the nature of the measurement. However, SAXS is one of the best techniques to directly assess conformational flexibility. Our scattering data for RsbU have multiple signatures of flexibility supporting a high confidence conclusion. While the scattering data support a reduction in flexibility for the RsbT/RsbU complex, we agree that a high resolution structure would be valuable. However the combination of the scattering data with our biochemical and genetic data supports the validity of the AlphaFold predicted model. We thank the reviewer for the suggestion of future hydrogen/deuterium exchange experiments that would be complementary, but which we feel are beyond the scope of this work.

> *The interpretation of the computed structure models should be toned down with the addition of a few caveats related to the bias in the models returned by AlphaFold2. For the full-length models of RsbU and other phosphatase proteins, the relationship of the domains to each other is likely to be the least reliable part of the models - this is apparent from the PAE plots shown in Supplementary Figure 8. Furthermore, the authors should show models coloured by pLDDT scores in an additional supplementary figure to help the reader interpret the confidence level of the predicted structures.*

We thank the reviewer for suggestions on how to clarify the discussion of AlphaFold models. We will decrease the emphasis on the computed models in the text and will add figures with the models colored by the pLDDT scores to aid in the interpretation.

We have modified the text of the Abstract: “This coiled-coil linker transduction mechanism additionally suggests a resolution to the mystery of how shared sensory domains control serine/threonine phosphatases, diguanylate cyclases and histidine kinases.”

We have modified the text of the Results: “These predictions suggest a testable hypothesis that RsbP is controlled through an activation mechanism similar to that of RsbU (Fig. 5A).”

“From this analysis, we speculate that linker-mediated phosphatase domain dimerization is an evolutionarily conserved, adaptable mechanism to control PPM phosphatase activity”

We have also added Figure 1 – figure supplement 2 with the AlphaFold2 models colored by the pLDDT scores.

> ***Recommendations for the authors:***
>
> ***Reviewer #1 (Recommendations for the authors):***
>
> *Baral and colleagues investigate the regulatory mechanisms of the General Stress Response (GSR) in Bacillus subtilis, focusing on the phosphatase RsbU and its regulation by the protein RsbT. The GSR is a critical adaptive mechanism that allows bacteria to survive under various stress conditions by reshaping their physiology through a broad transcriptional response. RsbU, a key player in the GSR, facilitates the activation of the transcription factor SigB by dephosphorylating RsbV. This activation is mediated through a partner-switching mechanism involving RsbT. Baral and colleagues use a combination of genetic screening, structural predictions via AlphaFold2, and biophysical techniques such as SAXS and MALS to present a model for how RsbT regulates RsbU. Key findings include the identification of specific amino acid substitutions that enhance RsbU activity, the role of the α-helical linker in RsbU dimerization and activation, and the potential broader conservation of these mechanisms across bacterial species. However, as described below, additional work is required to solidify the results.*
>
> *Major Points*
>
> *(1) The manuscript is misnamed--it dissects a single step of the signal-transduction pathway regulating the general stress response. Instead, it is rather seeking a generalizable mechanism for kinase -phosphatase interactions across stresses.*

We have edited the title to “A General Mechanism for Initiating the General Stress Response in Bacteria” to reflect that that this study addresses the initiating event of the general stress response.

> *(2) The genetic screen likely has limitations in detecting all possible variants that could affect RsbU activity. The readout is specific to σ^B activation, and the focus on specific amino acid substitutions may overlook other significant regions or mechanisms involved in the regulation of RsbU, particularly those involving RsbV and RsbT.*

Our screens were specifically designed to identify features of RsbU that contribute to regulation. Importantly, RsbU does not have any known targets other than RsbV and the downstream σ^B response but agree that substitutions in either RsbV or RsbT could influence RsbU activation. In principle our suppressor screen with $RsbU^{Y28I}$ could have identified RsbT variants (*rsbT* was mutagenized in this screen), but we did not identify any such variants in the screen. We conducted a separate screen (published elsewhere) that specifically addressed how RsbU recognizes RsbV.

> *(3) The authors largely focus on the biochemical and structural aspects of RsbU regulation. There is limited discussion on the broader functional implications of these*

> *findings in the context of bacterial physiology and stress response. Incorporating more in vivo studies to show how these mechanisms impact bacterial survival and adaptation would provide a more comprehensive understanding.*

We appreciate this comment, but did not conduct additional studies of survival and adaptation because the phenotypes of σ^B deletion in *B. subtilis* under laboratory conditions are relatively mild and therefore difficult to assay. Future studies to address this in other systems could be highly informative.

> *(4) The results primarily support the model of linker-mediated dimerization and rigidity. However, other potential regulatory mechanisms or interacting partners might also play significant roles in RsbU activation. A more thorough exploration of these possibilities would strengthen the study's conclusions.*

One of the major advantages of RsbU as a model for initiation of the general stress response is that the system is discreet with all evidence pointing to there being a single primary input (RsbT) and output (dephosphorylation of RsbV). While there are other possible variations on the system (for example RsbU may be directly activated by manganese stress), we focused on this system precisely because of its simplicity.

> *(5) While the study presents evidence for the conservation of the described mechanism across different species, this assumption is based on structural predictions and limited experimental data. Broader experimental validation across diverse bacterial species would be necessary to substantiate this claim. Coevolution coupling along with conservation/evolutionary studies could be considered.*

We have altered the language in the paper to emphasize where we are making inferences from predictions that are therefore more speculative. We agree that a more detailed analysis of the evolutionary coupling would likely be fruitful. We note that these couplings are the major driving force of AlphaFold predictions, suggesting that these couplings contributed to the models that we analyzed.

> *(6) The reliance on AlphaFold2 for structural predictions introduces potential biases and uncertainties inherent in computational models. Experimental validation of these models through additional techniques such as cryo-EM or X-ray crystallography would strengthen the conclusions.*

We agree with this point, which is why we performed extensive analysis and validation of the models for RsbU using SAXS, genetics, and biochemistry. The proposed techniques are made more challenging by flexibility and heterogeneity, which we detected in our experiments. Our attempts thus far at experimental structure determination are consistent with this being a major technical hurdle.

> *(7) SAXS data provide low-resolution structural information, and the interpretation of flexibility versus rigidification might be overemphasized in its interpretation. This part of the study was difficult to interpret. Improving readability by breaking down the text into sections with clear headings for each figure panel and clarifying descriptions of the panels and methods would help. Complementary high-resolution techniques could provide a more definitive view of the linker's conformational changes.*

We have modified the presentation of the figures to clarify the SAXS analysis. The fact that the SAXS analysis suggests flexibility rather than a discrete inactive conformation means that high-resolution techniques may not be appropriate for this system.

> *(8) The study primarily focuses on the model where RsbT binding rigidifies the RsbU linker. Alternative hypotheses, such as subtle conformational adjustments without complete rigidification, are not extensively explored or ruled out.*

Our analysis of the SAXS data strongly suggests that a subtle conformational change could not account for the scattering data that we obtained. We have modified the text to clarify this point.

"Indicative of significant deviation between the RsbU structure in solution to the AlphaFold2 model, the scattering intensity profile (I(q) vs. q) was a poor fit (χ^2 12.53) to a profile calculated from the AlphaFold2 model of an RsbU dimer using FoXS (Schneidman-Duhovny et al. 2016; Schneidman-Duhovny et al. 2013) (Fig. 4A). We therefore assessed the SAXS data for the RsbU dimer for features that report on flexibility (Kikhney & Svergun 2015). First, the scattering intensity data lacked distinct features caused by the multi-domain structure of RsbU from the AlphaFold2 model (Fig.4A)."

> *(9) Future studies should aim to validate the AlphaFold2 predictions with high-resolution structural techniques. This would provide definitive evidence for the proposed conformational states of RsbU with and without RsbT.*

The fact that the SAXS analysis suggests flexibility rather than a discrete inactive conformation means that high-resolution techniques may not be appropriate for this system.

> *(10) Investigating the RsbU-RsbT interaction in vivo using techniques like FRET, co-immunoprecipitation, or live-cell imaging would provide a more comprehensive understanding of their functional dynamics in a cellular context.*

We appreciate the reviewer's suggestions for future experiments.

> *(11) Exploring and testing alternative models of RsbU activation, such as partial rigidification or different modes of conformational change, would strengthen the conclusions.*

While our data strongly support that a flexible-to-rigid transition controls RsbU activation, we agree that it is possible that other mechanisms of linker modification could control other phosphatases and we discuss this at some length in the discussion.

> *(12) The figure legends are quite dense and could benefit from some streamlining.*

We have edited the figure legends for clarity and length.

> ***Reviewer #2 (Recommendations for the authors):***
>
> *(1) Activation assays (Figures 1, 3, S2) are presented here as blue or white spots (reflecting a reporter activity). While off and on these are fairly clear, it is more difficult to compare the degree of activity (for instance that rsbU^{Q94L} is more active than M166V). It would also be good to clearly present in the text the logic of asking if the mutant is RsbT independent or not (and the interpretation of that). Quantitative assays of these would be very useful.*

We chose not to perform quantitative-LacZ assays here because of several complications to interpreting these results that we encountered in our previously published study (Ho and Bradshaw, 2021). However, the level of blue pigmentation shown in Figure 1B for RsbU Q94L and RsbU M166V is qualitatively different, making the comparison possible. Most

importantly, we observed cell density dependent changes in LacZ activity in the absence of *rsbT* for $rsbU^{M166V}$ expressing cells, meaning that comparisons between strains would be difficult. Additionally, we found that it was important to make a chromosomal replacement of *rsbU* to see the full effect of the M166V substitution. However, we were not able to construct a similar $rsbU^{Q94L}$ strain, likely because the high level σ^B activity is lethal (we were able to construct this strain when σ^B was deleted but only obtained strains with additional loss-of-function mutations in RsbU when σ^B was present.

We have modified the text to explain the logic of identifying RsbT independent variants: "We previously conducted a genetic screen (Ho & Bradshaw 2021) to identify features of RsbU that are important for phosphatase regulation by isolating gain-of-function variants that are active in the absence of RsbT."

> *(2) Explain Figure S8 graphs: as much as Alphafold is now in use, the authors should provide some further explanation of what is shown here. Blue (low error) is good, presumably. What are the A, B, C, and D sections showing? Different parts of a given letter region (and between them)? What is the x-axis? Is the top-ranked model used in every case in the text? How different are these models? The Methods section could be used for some of this (but doesn't in its current form). This also becomes important for the models generated later in the paper (Figure S7), which look rather different here.*

We have modified figure S8 to include additional labels and have added structures with the pLDDT scores shown. We have additionally modified the figure legends and methods to provide the requested information.

> *(3) Figure 1C, D, Figure S2: amino acid ends of linker domains could be shown (text discusses 83-97 the linker as a two-turn coiled coil; Q94 is pretty close to the end of this coiled-coil? Figure S2 is even less clear - addresses of other amino acids would help, and or an added sequence showing the full linker and coiled-coil region). Some explanation for positions for readers to focus on for full coiled-coil would be useful in the legend of Figure S2. How strong a coiled-coil prediction is there for this region?*

We have added the sequence of the coiled-coil regions to the figures with numbering. For these analyses we used the Socket2 program, which analyzes a PDB file to identify coiled-coil regions and thus does not provide a confidence score. However, inspection of the sequence and the confidence scores of the AlphaFold2 models indicates that the coiled-coil regions are not ideal, consistent with this being a regulatory feature.

> *Is it clear that the fully inactive proteins are still properly folded and soluble?*

In the case of RsbU, our biophysical analysis indicates that the inactive form of the protein is soluble. While phosphatase activity is substantially reduced, our unpublished comparison of single- and multiple-turnover reactions in the absence of RsbT indicates that nearly all of the enzyme is active.

> *Finally, are there other positions that would also be expected, from this model, to stabilize the coiled-coil and thus bypass the requirement for RsbT? If so, it would be good to test these. Is it the burial of amino acid at position 94 that is important, or the ability to form crossed helices?*

Because of how short the predicted coiled-coil region is, we did not identify any obvious positions that would likely have the same effect as Q94 substitution. We considered making helix-breaking mutations, which would be predicted to block RsbU activation, but favored

analysis of the wildtype protein because of limitations in interpreting the effects of loss-of-function mutations.

> *(4) Figure 2A, RsbT binding to RsbU: It was not entirely clear to this reviewer why one would expect the RsbT binding, not needed for activation, to be increased by the mutation that stabilizes the crossed alpha helices. The change is impressive but doesn't the lack of a need for RsbT suggest that this mutation bypasses the normal mechanism? (Is dimerization enuf? Or other protein cross helices?).*

We have modified the text to clarify this point: “One prediction of our hypothesis that RsbT stabilizes the crossed alpha helices of the RsbU dimer, is that RsbT should bind more tightly to *rsbU*^{Q94L} than to *RsbU* because the coiled-coil conformation that RsbT binds would be more energetically favorable.” Another way of putting this is that if the Q94L substitution activates RsbU through an on-pathway mechanism, RsbT *must* bind more tightly.

> *(5) Figure 3A, Figure S3: Please label the yellow (interface) residues in RsbU and RsbT in Fig. S3 and the green (suppressor) spheres in Figure 3A.*

We have added labels to the figures as suggested.

> *If RbsT interacts with the N-terminal dimerization domain and linker, why were residues 174 and 178 (from PPM domain) shown to be implicated in binding?*

The fact that residues in the switch region suppress a mutation that decreases RsbT binding suggests that this region is part of an allosteric network that links RsbT binding, the linker, and dimerization of the phosphatase domains. For example, any substitution that promotes a conformation of the phosphatase domain that is more favorable for dimerization would also promote RsbT binding. However, the precise details of how each mutation fits into this network is not clear and we have therefore chosen to not specify a particular model to avoid over interpreting our data.

> *Are these marked in Figure S3?*

We have added labels to make this clear.

> *Are these part of a dimerization interface in the C-terminal domain? Are any/all of these RsbU mutants suppressed by Q94L, as one might predict (apparently Y28I is since Q94L was again identified)?*

We chose to focus on Y28I because it was the best studied previously, but we would predict that Q94L would suppress other RsbT binding mutations.

> *(6) Line 191-192: Is it surprising that no suppressors were isolated in RsbT?*

We didn’t have a preconception of whether or not it would be possible to identify similar suppressors in RsbT. Explanations for why we did not identify such suppressors could include that RsbT may be destabilized more easily by substitution, that RsbT is more constrained because it has other interaction partners, or that the particular substitutions that would suppress Y28I are less common by the PCR mutagenesis strategy we used.

> *(7) Figure 3: Would the same mutants arise if the screen had been done in the absence of RsbT? Was RsbT-dependent tested for the rsbU alleles?*

Our prediction is that we would not have identified any of these mutations except for Q94L in the absence of *rsbT*. We tested a few of the alleles and found them all to be *rsbT* dependent, but did not systematically test all of the alleles and therefore did not include this analysis in the manuscript.

> *Given the findings earlier in the paper for Q94L, suggesting that this stabilizes the coiled-coil and shows some activity in the absence of RsbT, it seems that the interpretation of other mutants in this region (and Q94L itself) as evidence that RsbT contacts the linker directly and that contact is necessary for activation may be an overinterpretation. If these are in fact RsbT independent, they support the importance of the linker (do they further stabilize coiled-coil formation?), rather than the role of RsbT here. Are G92 and T89 on the outside of the coiled-coil? If Q94 is buried, is it qualitatively different from these others?*

G92 and T89 are predicted to be exposed. The fact that these mutations are near Q94 is part of the reason that we focused on R91 and the predicted contact with D92 of RsbT as another approach to validate the predicted interface.

> *(8) Figure 3C addresses the issue of direct interaction of RsbT with the RsbU linker to some extent, given that RsbU R91E doesn't appear to have a lot of activity without RsbT. It would be helped by telling the reader what the R91 contact is initially.*

We have modified the text to clarify this point: “To test the model that RsbT activates RsbU by directly interacting with the linker to dimerize the RsbU phosphatase domains, we introduced a charge swap at position R91 that would abolish a predicted salt-bridge with RsbT D92 (Fig. 3C).”

> *(9) Figure 4 and the discussion of it in the text is not likely to be easily understandable for many readers. Aside from providing a bit more explanation of what these analyses are showing, it would be useful to start the whole section (or maybe even much earlier in the paper) with the information found on lines 261-264, that other studies show that the N-terminus dimerizes stably on its own (and is it known that the C-terminus does not?). Then the discussion of the alternative models early in this section would be clearer.*

We have updated the introduction to emphasize this point “RsbU has an N-terminal four-helix bundle domain that dimerizes RsbU and is also the binding site for RsbT, which activates RsbU as a phosphatase (Fig. 1C,D) (Delumeau et al. 2004).”

We have also added clarification to the model presented at the beginning of this section: “A second possibility is that inactive RsbU is dimerized by the N-terminal domains but that the linkers of inactive RsbU are flexible and that the phosphatase domains only interact with each other when RsbT orders the linkers into a crossing conformation.”

> *Is the dimerization of the N-terminal domains previously determined similar/the same as what is seen in the AlphaFold models used here (or the AlphaFold dimerization derived primarily from that data?).*

Yes, the dimerization in the AlphaFold models matches closely to the published structure.

> *(10) Discussion and Figure 5: The final part of this work predicts AlphaFold models for a set of other phosphatases involved in initiating GSR across bacterial species, and suggests that linked-mediated phosphatase dimerization is the critical factor to activate the phosphatase. Clearly, this is the most speculative but interesting aspect of the paper. A number of possible questions are suggested by some of this:*

> *a. Do any of the activating mutants In RsbU and RsbP in the PPM domain (that apparently improve dimerization and thus activation) do a similar job in the other modeled proteins?*

This is an interesting question, but unfortunately most of these proteins have not been biochemically characterized. We highlight examples of RsbP and *E. coli* RssB for which similar activating mutations have been characterized.

> *b. The legend (Figure 5G) suggests that all of the linker combinations will be coiled-coils, but that they will undergo different types of activating (and dimerizing?) transitions. Is that in fact what is being proposed here?*

Yes, this is our working hypothesis.

> *c. If there is no dimerization (as noted, only weak dimerization has been reported for E. coli RssB), does that generalize the model to there are linkers and their structures are important? At the least, would the folding up of the E. coli RssB linker with antiadaptor binding be considered another mode of signal transduction or rather some sort of storage form?*

Interestingly, the *P. aeruginosa* RssB constitutively dimerizes, suggesting the *E. coli* is the outlier.

> *d. Would the "toolkit" model, in which different changes occur in the linker regions, suggest that the interacting proteins are going to be critical for the type of linker changes that will be important? Or something about the nature of the linkers themselves?*

This is an interesting question that we cannot yet answer. We have chosen to focus on the possible flexibility of this mechanism and anticipate that a variety of mechanisms will be used.

> *e. Given the extensive comparison to E. coli RssB, the authors might consider a figure to clarify the relative domain architecture, sequences that are akin to switch regions, and others important to the discussion here.*

We tried to highlight this in Figure 5C including coloring the regions similar to the switch regions.

> ***Reviewer #3 (Recommendations for the authors):***
>
> *Given the caveats noted above related to the reliability of computed structure models, I would recommend the authors make the following additions/modifications to their manuscript:*
>
> *(1) The authors should show alpha fold models coloured by pLDDT scores in an additional supplementary figure to help the reader interpret the confidence level of the predicted structures.*

We have added these models to figure 1 – figure supplement 2.

> *(2) Because of the points mentioned above the authors should tone down the generalisation relating to the activation mechanism of this family of phosphatases presented in the discussion.*

We have modified the paper throughout to emphasize where we are speculating.

https://doi.org/10.7554/eLife.100376.2.sa0